

# A fourth-order multi-scale computational method and its convergence analysis for composite Kirchhoff plates with microscopic periodic configurations

Hao Dong<sup>a,\*</sup>, Liqun Cao<sup>b</sup>

<sup>a</sup>*School of Mathematics and Statistics, Xidian University, Xi'an 710071, PR China*

<sup>b</sup>*LSEC, ICMSEC, Academy of Mathematics and Systems Science, Chinese Academy of Sciences, Beijing 100190, PR China*

---

## Abstract

The Kirchhoff plate model plays a vital role in modeling, computing and analyzing the mechanical behaviors of thin plate structures. This study propose a novel fourth-order multi-scale (FOMS) computational method for high-accuracy and efficient simulation of composite Kirchhoff plates with highly periodic heterogeneities. At first, two-scale asymptotic expansion theory is employed to establish the high-accuracy fourth-order multi-scale computation model with novel fourth-order correctors for composite Kirchhoff plates, which are governed by fourth-order partial differential equation (PDE) with periodically oscillatory and highly discontinuous coefficients. Then, the locally point-wise error analysis is derived to theoretically illustrate the local balance preserving of fourth-order multi-scale model enabling high-accuracy multi-scale computation. Furthermore, a global error estimation with an explicit order for fourth-order multi-scale solutions is first demonstrated under appropriate assumptions. In contrast to the second- and third-order multi-scale solutions, only the fourth-order one is capable of providing an explicit error order estimate. Additionally, an efficient numerical algorithm is developed to conduct high-accuracy simulation for heterogeneous plate structures. Extensive numerical examples are provided to confirm the theoretical results for the computational convergence and accuracy of the proposed method. This work offers a higher-order (fourth-order) multi-scale computa-

---

\*Corresponding author.

*Email address:* donghao@mail.nwpu.edu.cn (Hao Dong)

tional framework that enables robust simulation and high-accuracy analysis to composite Kirchhoff plates.

*Keywords:* Composite Kirchhoff plates, Fourth-order multi-scale model, Local balance preserving, Efficient numerical algorithm, Global error estimation

---

## 1. Introduction

The tremendous progress in composite materials has been a key driver of the rapid development of modern science and technology. Engineering structures made of composite materials are widely used in engineering fields such as aerospace, aviation, marine, civil engineering, and architecture, etc. Particularly noteworthy are composite thin plate structures, whose mechanical properties-lightweight, high strength, and high reliability-have made them a focus of increased attention and application in the past few decades [1]. However, highly heterogeneous micro-structures of composite thin plates lead to tremendous cost to the high-accuracy modeling and simulation by use of classical numerical methods. Therefore, the development of high-accuracy and efficient numerical method is of paramount importance for effectively simulating the mechanical behaviors of composite thin plates.

In recent decades, scientists and engineers have developed a diverse array of multi-scale methods to overcome the challenging issues inherent in the multi-scale spatial nature of composite structures, such as asymptotic homogenization method (AHM) [2, 3], multi-scale finite element method (MsFEM) [4, 5], heterogeneous multi-scale method (HMM) [6], variational multi-scale method (VMS) [7], multi-scale eigenelement method (MEM) [8], localized orthogonal decomposition method (LOD) [9] and their improved versions [10, 11], among which the AHM is a quintessential approach with rigorous mathematical foundation and can balance the accuracy and efficiency of computational performance. Nevertheless, Cui and his research team revealed, via both theoretical analysis and engineering computation, the inadequate accuracy of classical AHM for highly heterogeneous composites. In the past thirty years, Cui and his research team systematically established a class of higher-order multi-scale approaches for precisely and efficiently simulating the thermal, mechanical and multiphysics behaviors of composite structures, as shown in references [12, 13, 14, 15, 16]. However, most of multi-scale approaches was primarily confined to simulate and analyze

the two-dimensional (2D) or three-dimensional (3D) multi-scale problems of composite structures, which are governed by second-order partial differential equation in spatial scale. These multi-scale methods can not directly apply to simulate the bending behaviors of composite thin plates with highly periodic heterogeneities, which are modeled by fourth-order partial differential equation named as Kirchhoff plate model [1]. The Kirchhoff plate is a classical plate model in which only deflection is the dependent variable, which is suitable for analyzing and simulating the thin plates, and widely employed in various engineering fields. Hence, the development of effective multi-scale computational methods for composite thin plates holds significant scientific importance and practical engineering value.

To the best of our knowledge, some progress has been achieved regarding the problems of composite thin plates, both in mathematical theory and numerical computation. From a mathematics theory perspective, Pastukhova established G-convergence theory for higher-order elliptic operators without considering boundary condition [17]. Pastukhova employed the shift method to prove the operator error estimates for fourth-order elliptic equations in the unbounded domain without considering boundary condition [18]. Moreover, researcher derived the operator error estimates of the Dirichlet and Neumann problems for higher-order elliptic equations with periodic coefficients in the bounded domain [19, 20]. In addition, Niu et al. established the quantitative error estimates in homogenization and almost-periodic of higher-order elliptic systems [21, 22, 23]. Nevertheless, the aforementioned theoretical findings are not established on the basis of the plate model in practical engineering applications, and without effective numerical algorithms. In recent years, Xing et al. developed a two-scale asymptotic homogenization method for composite Kirchhoff plates with periodic micro-structures and obtained the two-scale convergence results for the two-scale asymptotic expansion solution with second-order corrector [24, 25]. However, the proposed homogenization method fails to capture the highly oscillatory behavior in the composite Kirchhoff plates with high fidelity. And also, the proposed two-scale convergence results are deficient in that they do not offer a quantitative error estimate. From a computational method perspective, some analytical approaches have been developed to obtain the effective mechanical parameters of composite plates [1, 26, 27, 28]. However, these analytical approaches are not suitable for composite plates with complicated microscopic configurations. Additionally, researchers developed a novel numerical implementation of asymptotic homogenization method to predict effective

properties of periodic plates without any complicated mathematical derivation [29]. In reference [30], a consistent multi-scale formulation is presented for the bending analysis of heterogeneous thin plate structures containing three dimensional reinforcements with in-plane periodicity. Thus a unified numerical implementation for thin plate analysis can be conveniently realized using the triangular elements with discretization flexibility and the quadratic Hermite triangular element with improved accuracy. Moreover, based on the theoretical framework of the extended multi-scale finite element method, an efficient multi-scale finite element method is developed for small-deflection analysis of thin composite plates with aperiodic microstructure characteristics [31]. Aliabadi et al. presented a novel approach to concurrent multi-scale analysis, which employed a plate model to formulate structures at both scales, and homogenisation was performed using the FFT-based approach, offering higher efficiency compared to conventional methods [32]. However, the aforementioned proposed approaches in references [24, 29, 30, 31, 32] are limited in their inability to implement high-accuracy simulation of composite plates with high-contrast material properties, and they are not equipped with a quantitative and explicit error estimate.

In this work, an innovative fourth-order multi-scale method is presented for high-accuracy and efficient simulation of fourth-order composite Kirchhoff plate problems. The pivotal contributions of this work are summarized as three pillars. (1) The fourth-order multi-scale computational model with novel fourth-order correctors is presented, which can preserve the local balance of transverse loads enabling high-resolution capturing of locally high-frequency oscillatory behavior in composite Kirchhoff plates. (2) The explicit error estimate for fourth-order multi-scale solution for fourth-order multi-scale PDE is derived for the first time, that provides a quantitative convergence rate for fourth-order multi-scale solution. (3) The efficient numerical algorithm is developed for effective multi-scale simulation of composite plate bending problems, thereby providing a robust numerical framework for real-world engineering applications.

The organization of this study is as follows. In Section 2, the establishment of fourth-order multi-scale computational model for composite Kirchhoff plates is introduced in detail. Section 3 conduct both local and global error analyses for multi-scale asymptotic solutions in the point-wise and energy senses. In particular, the explicit error order for fourth-order multi-scale problems is obtained for the first time. In Section 4, a high-accuracy and efficient numerical algorithm is developed to effectively simulate the bend-

ing problems of Kirchhoff plates with microscopic periodic configurations. In Section 5, numerical experiments are carried out to verify the computational performance of the proposed FOMS method including FOMS model and corresponding numerical algorithm. Eventually, concluding remarks and potential directions are drawn in Section 6. Throughout this paper, Einstein summation convention is utilized to streamline repetitive indices.

## 2. Fourth-order multi-scale computational model for composite Kirchhoff plates

### 2.1. The mathematical setting of composite Kirchhoff plates

Based on the classical plate theory in [1, 33, 34], the following fourth-order partial differential equation with rapidly oscillating and highly discontinuous coefficients is presented for composite Kirchhoff plates with spatial periodic heterogeneity.

$$\begin{cases} \frac{\partial^2}{\partial x_i \partial x_j} \left[ D_{ijkl}^\epsilon(\mathbf{x}) \frac{\partial^2 \omega^\epsilon(\mathbf{x})}{\partial x_k \partial x_l} \right] = q(\mathbf{x}), & \text{in } \Omega, \\ \omega^\epsilon(\mathbf{x}) = g_1(\mathbf{x}), & \text{on } \partial\Omega, \\ \frac{\partial \omega^\epsilon(\mathbf{x})}{\partial x_j} \hat{n}_j = g_2(\mathbf{x}), & \text{on } \partial\Omega, \end{cases} \quad (1)$$

where  $\Omega$  denotes a bounded convex domain in  $\mathbb{R}^2$  with a Lipschitz continuous boundary  $\partial\Omega$ .  $D_{ijkl}^\epsilon(\mathbf{x})$  is the fourth-order bending stiffness tensor.  $\omega^\epsilon(\mathbf{x})$  denotes the undetermined transverse displacement on the reference middle surface of composite Kirchhoff plates, where the superscript  $\epsilon$  represents the characteristic length of periodic unit cell (PUC) in composite Kirchhoff plates.  $q(\mathbf{x})$  denotes the transverse load imposed on composite Kirchhoff plates.  $g_1(\mathbf{x})$  and  $g_2(\mathbf{x})$  denote the prescribed transverse displacement and the prescribed in-plane rotation on domain boundary  $\Omega$ . Besides, without loss of generality,  $\mathbf{n} = (\hat{n}_1, \hat{n}_2)$  denotes the outward normal vector on the outer boundary  $\partial\Omega$ .

In accordance with multi-scale homogenization theory, we can define microscopic variable  $\mathbf{y} = \mathbf{x}/\epsilon = (x_1/\epsilon, x_2/\epsilon) = (y_1, y_2)$  for periodic unit cell  $\mathbf{Y} = [0, 1]^2$ . Consequently, material parameter  $D_{ijkl}^\epsilon(\mathbf{x})$  can be formulated as new form  $D_{ijkl}(\mathbf{y})$ , which necessitate this material parameter is 1-periodic function in variable  $\mathbf{y}$ . To implement the subsequent multi-scale modeling and theoretical analysis, this section starts with the following assumptions for the above fourth-order governing PDE (1).

- (A<sub>1</sub>) The bending stiffness coefficient  $D_{ijkl}^\epsilon(\mathbf{x}) \in L^\infty(\Omega)$ .  
(A<sub>2</sub>) Function  $D_{ijkl}^\epsilon(\mathbf{x})$  is symmetric and uniform ellipticity, and there exist two constants  $0 < \alpha \leq \beta$  such that,

$$D_{ijkl}^\epsilon = D_{ijlk}^\epsilon = D_{klji}^\epsilon, \quad \alpha \eta_{ij} \eta_{ij} \leq D_{ijkl}^\epsilon(\mathbf{x}) \eta_{ij} \eta_{kl} \leq \beta \eta_{ij} \eta_{ij},$$

for arbitrary symmetric matrix  $\{\eta_{ij}\} \in \mathbb{R}^{2 \times 2}$ .

- (A<sub>3</sub>) Function  $q(\mathbf{x}) \in H^{-2}(\Omega)$ , function  $g_1(\mathbf{x}) \in H^{3/2}(\partial\Omega)$ , function  $g_2(\mathbf{x}) \in H^{1/2}(\partial\Omega)$ .

## 2.2. Higher-order multi-scale analysis for composite Kirchhoff plates

Firstly, taking into account the microscopic periodicity and scale separation of composite plates, the following multi-scale chain rules can be determined for subsequent multi-scale modeling.

$$\frac{\partial \Phi^\epsilon(\mathbf{x})}{\partial x_i} = \frac{\partial \Phi(\mathbf{x}, \mathbf{y})}{\partial x_i} + \frac{1}{\epsilon} \frac{\partial \Phi(\mathbf{x}, \mathbf{y})}{\partial y_i}, \quad (2)$$

$$\frac{\partial^2 \Phi^\epsilon(\mathbf{x})}{\partial x_i \partial x_j} = \frac{\partial^2 \Phi(\mathbf{x}, \mathbf{y})}{\partial x_i \partial x_j} + \frac{1}{\epsilon} \frac{\partial^2 \Phi(\mathbf{x}, \mathbf{y})}{\partial x_i \partial y_j} + \frac{1}{\epsilon} \frac{\partial^2 \Phi(\mathbf{x}, \mathbf{y})}{\partial y_i \partial x_j} + \frac{1}{\epsilon^2} \frac{\partial^2 \Phi(\mathbf{x}, \mathbf{y})}{\partial y_i \partial y_j}. \quad (3)$$

To clarify and simplify subsequent multi-scale analysis, a series of differential operators is defined according to the aforementioned chain rules as follows.

$$\left\{ \begin{array}{l} B_0 \omega^\epsilon(\mathbf{x}) = \frac{\partial^2}{\partial y_i \partial y_j} \left[ D_{ijkl}(\mathbf{y}) \frac{\partial^2 \omega^\epsilon(\mathbf{x})}{\partial y_k \partial y_l} \right], \\ B_1 \omega^\epsilon(\mathbf{x}) = 2 \frac{\partial^2}{\partial x_i \partial y_j} \left[ D_{ijkl}(\mathbf{y}) \frac{\partial^2 \omega^\epsilon(\mathbf{x})}{\partial y_k \partial y_l} \right] + 2 \frac{\partial^2}{\partial y_i \partial y_j} \left[ D_{ijkl}(\mathbf{y}) \frac{\partial^2 \omega^\epsilon(\mathbf{x})}{\partial x_k \partial y_l} \right], \\ B_2 \omega^\epsilon(\mathbf{x}) = \frac{\partial^2}{\partial x_i \partial x_j} \left[ D_{ijkl}(\mathbf{y}) \frac{\partial^2 \omega^\epsilon(\mathbf{x})}{\partial y_k \partial y_l} \right] + \frac{\partial^2}{\partial y_i \partial y_j} \left[ D_{ijkl}(\mathbf{y}) \frac{\partial^2 \omega^\epsilon(\mathbf{x})}{\partial x_k \partial x_l} \right] \\ \quad + 4 \frac{\partial^2}{\partial x_i \partial y_j} \left[ D_{ijkl}(\mathbf{y}) \frac{\partial^2 \omega^\epsilon(\mathbf{x})}{\partial x_k \partial y_l} \right], \\ B_3 \omega^\epsilon(\mathbf{x}) = 2 \frac{\partial^2}{\partial y_i \partial x_j} \left[ D_{ijkl}(\mathbf{y}) \frac{\partial^2 \omega^\epsilon(\mathbf{x})}{\partial x_k \partial x_l} \right] + 2 \frac{\partial^2}{\partial x_i \partial x_j} \left[ D_{ijkl}(\mathbf{y}) \frac{\partial^2 \omega^\epsilon(\mathbf{x})}{\partial y_k \partial x_l} \right], \\ B_4 \omega^\epsilon(\mathbf{x}) = \frac{\partial^2}{\partial x_i \partial x_j} \left[ D_{ijkl}(\mathbf{y}) \frac{\partial^2 \omega^\epsilon(\mathbf{x})}{\partial x_k \partial x_l} \right]. \end{array} \right. \quad (4)$$

Next, assume that the transverse displacement solution  $\omega^\epsilon(\mathbf{x})$  of the fourth-order PDE (1) has the following asymptotic expansion form.

$$\begin{cases} \omega^\epsilon(\mathbf{x}) = \omega^{(0)}(\mathbf{x}, \mathbf{y}) + \epsilon \omega^{(1)}(\mathbf{x}, \mathbf{y}) + \epsilon^2 \omega^{(2)}(\mathbf{x}, \mathbf{y}) \\ \quad + \epsilon^3 \omega^{(3)}(\mathbf{x}, \mathbf{y}) + \epsilon^4 \omega^{(4)}(\mathbf{x}, \mathbf{y}) + O(\epsilon^5). \end{cases} \quad (5)$$

And also, substituting multi-scale asymptotic form (5) into multi-scale PDE (1), and utilizing the chain rules and differential operators provided in (2)-(4) gives the following series of equations by grouping the power-like terms of small periodic parameter  $\epsilon$ .

$$O(\epsilon^{-4}) : B_0 \omega^{(0)}(\mathbf{x}, \mathbf{y}) = 0. \quad (6)$$

$$O(\epsilon^{-3}) : B_0 \omega^{(1)}(\mathbf{x}, \mathbf{y}) + B_1 \omega^{(0)}(\mathbf{x}, \mathbf{y}) = 0. \quad (7)$$

$$O(\epsilon^{-2}) : B_0 \omega^{(2)}(\mathbf{x}, \mathbf{y}) + B_1 \omega^{(1)}(\mathbf{x}, \mathbf{y}) + B_2 \omega^{(0)}(\mathbf{x}, \mathbf{y}) = 0. \quad (8)$$

$$O(\epsilon^{-1}) : B_0 \omega^{(3)}(\mathbf{x}, \mathbf{y}) + B_1 \omega^{(2)}(\mathbf{x}, \mathbf{y}) + B_2 \omega^{(1)}(\mathbf{x}, \mathbf{y}) + B_3 \omega^{(0)}(\mathbf{x}, \mathbf{y}) = 0. \quad (9)$$

$$\begin{aligned} O(\epsilon^0) : & B_0 \omega^{(4)}(\mathbf{x}, \mathbf{y}) + B_1 \omega^{(3)}(\mathbf{x}, \mathbf{y}) + B_2 \omega^{(2)}(\mathbf{x}, \mathbf{y}) \\ & + B_3 \omega^{(1)}(\mathbf{x}, \mathbf{y}) + B_4 \omega^{(0)}(\mathbf{x}, \mathbf{y}) = q(\mathbf{x}). \end{aligned} \quad (10)$$

According to the  $O(\epsilon^{-4})$ -order equation (6), we find that  $\omega^{(0)}$  is independent of the microscopic variable  $\mathbf{y}$ , i.e.

$$\omega^{(0)}(\mathbf{x}, \mathbf{y}) = \omega^{(0)}(\mathbf{x}). \quad (11)$$

Thus  $\omega^{(0)}(\mathbf{x})$  is called as macroscopic homogenized solution.

From the definition of  $\omega^{(0)}(\mathbf{x})$ , we can reduce the  $O(\epsilon^{-3})$ -order equation (7) to the following equation.

$$B_0 \omega^{(1)}(\mathbf{x}, \mathbf{y}) = 0. \quad (12)$$

After that, based on equation (12) and the periodicity of function  $\omega^{(1)}(\mathbf{x}, \mathbf{y})$  in microscopic variable  $\mathbf{y}$ , it is clear that we have the following.

$$\omega^{(1)}(\mathbf{x}, \mathbf{y}) = 0, \quad (13)$$

Combining the conclusions of (11) and (13), we can simplify the  $O(\epsilon^{-2})$ -order equation (8) as the following equation.

$$\frac{\partial^2}{\partial y_i \partial y_j} \left[ D_{ijkl}(\mathbf{y}) \frac{\partial^2 \omega^{(2)}(\mathbf{x}, \mathbf{y})}{\partial y_k \partial y_l} \right] = - \frac{\partial^2 D_{ij\alpha_1\alpha_2}(\mathbf{y})}{\partial y_i \partial y_j} \frac{\partial^2 \omega^{(0)}(\mathbf{x})}{\partial x_{\alpha_1} \partial x_{\alpha_2}}. \quad (14)$$

In virtue of the governing equation (14) concerning  $\omega^{(2)}(\mathbf{x}, \mathbf{y})$ , we can define the following particular separation-of-variable form for  $\omega^{(2)}(\mathbf{x}, \mathbf{y})$

$$\omega^{(2)}(\mathbf{x}, \mathbf{y}) = \mathcal{N}_2^{\alpha_1 \alpha_2}(\mathbf{y}) \frac{\partial^2 \omega^{(0)}(\mathbf{x})}{\partial x_{\alpha_1} \partial x_{\alpha_2}}, \quad (15)$$

where  $\mathcal{N}_2^{\alpha_1 \alpha_2}(\mathbf{y})$  denotes the second-order cell functions. Moreover, substituting (15) into (14), the following equations are derived for solving  $\mathcal{N}_2^{\alpha_1 \alpha_2}(\mathbf{y})$  by attaching clamped boundary condition.

$$\begin{cases} \frac{\partial^2}{\partial y_i \partial y_j} \left[ D_{ijkl}(\mathbf{y}) \frac{\partial^2 \mathcal{N}_2^{\alpha_1 \alpha_2}(\mathbf{y})}{\partial y_k \partial y_l} \right] = -\frac{\partial^2 D_{ij\alpha_1 \alpha_2}(\mathbf{y})}{\partial y_i \partial y_j}, & \mathbf{y} \in \mathbf{Y}, \\ \mathcal{N}_2^{\alpha_1 \alpha_2}(\mathbf{y}) = 0, & \mathbf{y} \in \partial \mathbf{Y}, \\ \frac{\partial \mathcal{N}_2^{\alpha_1 \alpha_2}(\mathbf{y})}{\partial y_j} \hat{n}_j = 0, & \mathbf{y} \in \partial \mathbf{Y}. \end{cases} \quad (16)$$

Furthermore, together with the facts (11), (13) and (15), the  $O(\epsilon^{-1})$ -order equation (9) can be naturally reduced to the following equation.

$$\begin{aligned} \frac{\partial^2}{\partial y_i \partial y_j} \left[ D_{ijkl}(\mathbf{y}) \frac{\partial^2 \omega^{(3)}(\mathbf{x}, \mathbf{y})}{\partial y_k \partial y_l} \right] &= -2 \frac{\partial}{\partial y_j} \left[ D_{\alpha_1 jkl}(\mathbf{y}) \frac{\partial^2 \mathcal{N}_2^{\alpha_2 \alpha_3}(\mathbf{y})}{\partial y_k \partial y_l} \right] \frac{\partial^3 \omega^{(0)}(\mathbf{x})}{\partial x_{\alpha_1} \partial x_{\alpha_2} \partial x_{\alpha_3}} \\ &- 2 \frac{\partial^2}{\partial y_i \partial y_j} \left[ D_{ij\alpha_1 l}(\mathbf{y}) \frac{\partial \mathcal{N}_2^{\alpha_2 \alpha_3}(\mathbf{y})}{\partial y_l} \right] \frac{\partial^3 \omega^{(0)}(\mathbf{x})}{\partial x_{\alpha_1} \partial x_{\alpha_2} \partial x_{\alpha_3}} - 2 \frac{\partial D_{i\alpha_1 \alpha_2 \alpha_3}(\mathbf{y})}{\partial y_i} \frac{\partial^3 \omega^{(0)}(\mathbf{x})}{\partial x_{\alpha_1} \partial x_{\alpha_2} \partial x_{\alpha_3}}. \end{aligned} \quad (17)$$

According to (17), the same technique to define (15) suggests  $\omega^{(3)}(\mathbf{x}, \mathbf{y})$  can be expressed in a separation-of-variable form as below.

$$\omega^{(3)}(\mathbf{x}, \mathbf{y}) = \mathcal{N}_3^{\alpha_1 \alpha_2 \alpha_3}(\mathbf{y}) \frac{\partial^3 \omega^{(0)}(\mathbf{x})}{\partial x_{\alpha_1} \partial x_{\alpha_2} \partial x_{\alpha_3}}, \quad (18)$$

where  $\mathcal{N}_3^{\alpha_1 \alpha_2 \alpha_3}(\mathbf{y})$  denotes the third-order cell functions. Again, substituting (18) into (17), we can obtain the governing equations for solving  $\mathcal{N}_3^{\alpha_1 \alpha_2 \alpha_3}(\mathbf{y})$  by applying clamped boundary condition.

$$\begin{cases} \frac{\partial^2}{\partial y_i \partial y_j} \left[ D_{ijkl}(\mathbf{y}) \frac{\partial^2 \mathcal{N}_3^{\alpha_1 \alpha_2 \alpha_3}(\mathbf{y})}{\partial y_k \partial y_l} \right] = -2 \frac{\partial}{\partial y_j} \left[ D_{\alpha_1 jkl}(\mathbf{y}) \frac{\partial^2 \mathcal{N}_2^{\alpha_2 \alpha_3}(\mathbf{y})}{\partial y_k \partial y_l} \right] \\ \quad - 2 \frac{\partial^2}{\partial y_i \partial y_j} \left[ D_{ij\alpha_1 l}(\mathbf{y}) \frac{\partial \mathcal{N}_2^{\alpha_2 \alpha_3}(\mathbf{y})}{\partial y_l} \right] - 2 \frac{\partial D_{i\alpha_1 \alpha_2 \alpha_3}(\mathbf{y})}{\partial y_i}, & \mathbf{y} \in \mathbf{Y}, \\ \mathcal{N}_3^{\alpha_1 \alpha_2 \alpha_3}(\mathbf{y}) = 0, & \mathbf{y} \in \partial \mathbf{Y}, \\ \frac{\partial \mathcal{N}_3^{\alpha_1 \alpha_2 \alpha_3}(\mathbf{y})}{\partial y_j} \hat{n}_j = 0, & \mathbf{y} \in \partial \mathbf{Y}. \end{cases} \quad (19)$$



Subsequently, performing an integral on both sides of the  $O(\epsilon^0)$ -order equation (10) over PUC  $\mathbf{Y}$ , exploiting the Gauss theorem on equation (10) and replacing herein  $\omega^{(2)}$  by its formula (15) simultaneously, these procedures lead to derive the macroscopic homogenized equation for composite Kirchhoff plates as follows.

$$\begin{cases} -\frac{\partial^2}{\partial x_i \partial x_j} \left[ \hat{D}_{ijkl} \frac{\partial^2 \omega^{(0)}(\mathbf{x})}{\partial x_k \partial x_l} \right] = q(\mathbf{x}), & \text{in } \Omega, \\ \omega^{(0)}(\mathbf{x}) = g_1(\mathbf{x}), & \text{on } \partial\Omega, \\ \frac{\partial \omega^{(0)}(\mathbf{x})}{\partial x_j} \hat{n}_j = g_2(\mathbf{x}), & \text{on } \partial\Omega, \end{cases} \quad (20)$$

where the homogenized bending stiffness parameters  $\hat{D}_{ijkl}$  can be evaluated by the following formula.

$$\hat{D}_{ijkl} = \frac{1}{|\mathbf{Y}|} \int_{\mathbf{Y}} \left[ D_{ijkl}(\mathbf{y}) + D_{ij\alpha_1\alpha_2}(\mathbf{y}) \frac{\partial^2 \mathcal{N}_2^{kl}(\mathbf{y})}{\partial y_{\alpha_1} \partial y_{\alpha_2}} \right] d\mathbf{Y}. \quad (21)$$

Now, we initiate to establish the crucial fourth-order corrector  $\omega^{(4)}(\mathbf{x}, \mathbf{y})$ . By inserting the particular expressions (11), (13), (15) and (18) into equation (10), and replacing  $q(\mathbf{x})$  in equation (10) with its equivalent definition in macroscopic homogenized equation (20), we can reduce the  $O(\epsilon^0)$ -order equation (10) as the following equation.

$$\begin{aligned} \frac{\partial^2}{\partial y_i \partial y_j} \left[ D_{ijkl}(\mathbf{y}) \frac{\partial^2 \omega^{(4)}(\mathbf{x}, \mathbf{y})}{\partial y_k \partial y_l} \right] &= \hat{D}_{\alpha_1\alpha_2\alpha_3\alpha_4} \frac{\partial^4 \omega^{(0)}(\mathbf{x})}{\partial x_{\alpha_1} \partial x_{\alpha_2} \partial x_{\alpha_3} \partial x_{\alpha_4}} \\ &- D_{\alpha_1\alpha_2\alpha_3\alpha_4}(\mathbf{y}) \frac{\partial^4 \omega^{(0)}(\mathbf{x})}{\partial x_{\alpha_1} \partial x_{\alpha_2} \partial x_{\alpha_3} \partial x_{\alpha_4}} - 2 \frac{\partial}{\partial y_j} \left[ D_{\alpha_1 j k l}(\mathbf{y}) \frac{\partial^2 \mathcal{N}_3^{\alpha_2\alpha_3\alpha_4}(\mathbf{y})}{\partial y_k \partial y_l} \right] \frac{\partial^4 \omega^{(0)}(\mathbf{x})}{\partial x_{\alpha_1} \partial x_{\alpha_2} \partial x_{\alpha_3} \partial x_{\alpha_4}} \\ &- 2 \frac{\partial^2}{\partial y_i \partial y_j} \left[ D_{ij\alpha_1 l}(\mathbf{y}) \frac{\partial \mathcal{N}_3^{\alpha_2\alpha_3\alpha_4}(\mathbf{y})}{\partial y_l} \right] \frac{\partial^4 \omega^{(0)}(\mathbf{x})}{\partial x_{\alpha_1} \partial x_{\alpha_2} \partial x_{\alpha_3} \partial x_{\alpha_4}} \\ &- D_{\alpha_1\alpha_2 k l}(\mathbf{y}) \frac{\partial^2 \mathcal{N}_2^{\alpha_3\alpha_4}(\mathbf{y})}{\partial y_k \partial y_l} \frac{\partial^4 \omega^{(0)}(\mathbf{x})}{\partial x_{\alpha_1} \partial x_{\alpha_2} \partial x_{\alpha_3} \partial x_{\alpha_4}} - \frac{\partial^2}{\partial y_i \partial y_j} \left[ D_{ij\alpha_1\alpha_2}(\mathbf{y}) \mathcal{N}_2^{\alpha_3\alpha_4}(\mathbf{y}) \right] \frac{\partial^4 \omega^{(0)}(\mathbf{x})}{\partial x_{\alpha_1} \partial x_{\alpha_2} \partial x_{\alpha_3} \partial x_{\alpha_4}} \\ &- 4 \frac{\partial}{\partial y_j} \left[ D_{\alpha_1 j \alpha_2 l}(\mathbf{y}) \frac{\partial \mathcal{N}_2^{\alpha_3\alpha_4}(\mathbf{y})}{\partial y_l} \right] \frac{\partial^4 \omega^{(0)}(\mathbf{x})}{\partial x_{\alpha_1} \partial x_{\alpha_2} \partial x_{\alpha_3} \partial x_{\alpha_4}}. \end{aligned} \quad (22)$$

As observed in equation (22), we can establish the separation-of-variable

expression for  $\omega^{(4)}(\mathbf{x}, \mathbf{y})$  as follows.

$$\omega^{(4)}(\mathbf{x}, \mathbf{y}) = \mathcal{N}_4^{\alpha_1 \alpha_2 \alpha_3 \alpha_4}(\mathbf{y}) \frac{\partial^4 \omega^{(0)}(\mathbf{x})}{\partial x_{\alpha_1} \partial x_{\alpha_2} \partial x_{\alpha_3} \partial x_{\alpha_4}}, \quad (23)$$

where  $\mathcal{N}_4^{\alpha_1 \alpha_2 \alpha_3 \alpha_4}(\mathbf{y})$  denotes the fourth-order cell functions. Moreover, substituting (23) into (22), one can deduce the following governing equation for computing  $\mathcal{N}_4^{\alpha_1 \alpha_2 \alpha_3 \alpha_4}(\mathbf{y})$  by imposing clamped boundary condition.

$$\begin{cases} \frac{\partial^2}{\partial y_i \partial y_j} \left[ D_{ijkl}(\mathbf{y}) \frac{\partial^2 \mathcal{N}_4^{\alpha_1 \alpha_2 \alpha_3 \alpha_4}(\mathbf{y})}{\partial y_k \partial y_l} \right] = \widehat{D}_{\alpha_1 \alpha_2 \alpha_3 \alpha_4} - D_{\alpha_1 \alpha_2 \alpha_3 \alpha_4}(\mathbf{y}) \\ - 2 \frac{\partial}{\partial y_j} \left[ D_{\alpha_1 jkl}(\mathbf{y}) \frac{\partial^2 \mathcal{N}_3^{\alpha_2 \alpha_3 \alpha_4}(\mathbf{y})}{\partial y_k \partial y_l} \right] - 2 \frac{\partial^2}{\partial y_i \partial y_j} \left[ D_{ij\alpha_1 l}(\mathbf{y}) \frac{\partial \mathcal{N}_3^{\alpha_2 \alpha_3 \alpha_4}(\mathbf{y})}{\partial y_l} \right] \\ - D_{\alpha_1 \alpha_2 kl}(\mathbf{y}) \frac{\partial^2 \mathcal{N}_2^{\alpha_3 \alpha_4}(\mathbf{y})}{\partial y_k \partial y_l} - \frac{\partial^2}{\partial y_i \partial y_j} \left[ D_{ij\alpha_1 \alpha_2}(\mathbf{y}) \mathcal{N}_2^{\alpha_3 \alpha_4}(\mathbf{y}) \right] \\ - 4 \frac{\partial}{\partial y_j} \left[ D_{\alpha_1 j \alpha_2 l}(\mathbf{y}) \frac{\partial \mathcal{N}_2^{\alpha_3 \alpha_4}(\mathbf{y})}{\partial y_l} \right], \quad \mathbf{y} \in \mathbf{Y}, \\ \mathcal{N}_4^{\alpha_1 \alpha_2 \alpha_3 \alpha_4}(\mathbf{y}) = 0, \quad \mathbf{y} \in \partial \mathbf{Y}, \\ \frac{\partial \mathcal{N}_4^{\alpha_1 \alpha_2 \alpha_3 \alpha_4}(\mathbf{y})}{\partial y_j} \hat{n}_j = 0, \quad \mathbf{y} \in \partial \mathbf{Y}. \end{cases} \quad (24)$$

**Remark 1.** On the basis of Lax-Milgram theorem and the assumption  $(A_2)$ , the existence and uniqueness of solutions for auxiliary cell problems (16), (19) and (24) can be proved in [35, 36].

**Remark 2.** On the basis of Lax-Milgram theorem and the assumptions  $(A_2)$  and  $(A_3)$ , the existence and uniqueness of the macroscopic homogenized solution to the fourth-order homogenized PDE (20) can be proved.

Summing up, the above-mentioned multi-scale analysis can be concluded with the following theorem.

**Theorem 1.** The fourth-order multi-scale asymptotic solution of the plate bending problems of composite Kirchhoff plates is given as follows

$$\begin{aligned} \omega^{(4\epsilon)}(\mathbf{x}) = & \omega^{(0)}(\mathbf{x}) + \epsilon^2 \mathcal{N}_2^{\alpha_1 \alpha_2}(\mathbf{y}) \frac{\partial^2 \omega^{(0)}(\mathbf{x})}{\partial x_{\alpha_1} \partial x_{\alpha_2}} + \epsilon^3 \mathcal{N}_3^{\alpha_1 \alpha_2 \alpha_3}(\mathbf{y}) \frac{\partial^3 \omega^{(0)}(\mathbf{x})}{\partial x_{\alpha_1} \partial x_{\alpha_2} \partial x_{\alpha_3}} \\ & + \epsilon^4 \mathcal{N}_4^{\alpha_1 \alpha_2 \alpha_3 \alpha_4}(\mathbf{y}) \frac{\partial^4 \omega^{(0)}(\mathbf{x})}{\partial x_{\alpha_1} \partial x_{\alpha_2} \partial x_{\alpha_3} \partial x_{\alpha_4}}. \end{aligned} \quad (25)$$

According to the Kirchhoff plate theory, the displacement field of the composite plate for bending problems can be determined as follows.

$$u_1^\epsilon \approx u_1^{(4\epsilon)} = -x_3 \frac{\partial \omega^{(4\epsilon)}(\mathbf{x})}{\partial x_1} \quad (26)$$

$$u_2^\epsilon \approx u_2^{(4\epsilon)} = -x_3 \frac{\partial \omega^{(4\epsilon)}(\mathbf{x})}{\partial x_2} \quad (27)$$

$$u_3^\epsilon \approx \omega^{(4\epsilon)}(\mathbf{x}) \quad (28)$$

### 3. Theoretical error analysis of multi-scale asymptotic solutions

This section presents the theoretical error analysis of multi-scale asymptotic solutions for bending problems of composite Kirchhoff plates in the local and global senses in detail.

#### 3.1. Local error analysis in the point-wise sense

First define the second-order multi-scale solution and third-order multi-scale solution for composite Kirchhoff plates as below.

$$\omega^{(2\epsilon)} = \omega^{(0)} + \epsilon \omega^{(1)} + \epsilon^2 \omega^{(2)} = \omega^{(0)} + \epsilon^2 \omega^{(2)}. \quad (29)$$

$$\omega^{(3\epsilon)} = \omega^{(0)} + \epsilon \omega^{(1)} + \epsilon^2 \omega^{(2)} + \epsilon^3 \omega^{(3)} = \omega^{(0)} + \epsilon^2 \omega^{(2)} + \epsilon^3 \omega^{(3)}. \quad (30)$$

The fourth-order multi-scale solution  $\omega^{(4\epsilon)}$  is defined as formula (25).

Furthermore, define the following residual functions for different kinds of multi-scale solutions.

$$Z_\Delta^{(2\epsilon)}(\mathbf{x}) = \omega^\epsilon(\mathbf{x}) - \omega^{(2\epsilon)}(\mathbf{x}), \quad \mathbf{x} \in \Omega. \quad (31)$$

$$Z_\Delta^{(3\epsilon)}(\mathbf{x}) = \omega^\epsilon(\mathbf{x}) - \omega^{(3\epsilon)}(\mathbf{x}), \quad \mathbf{x} \in \Omega. \quad (32)$$

$$Z_\Delta^{(4\epsilon)}(\mathbf{x}) = \omega^\epsilon(\mathbf{x}) - \omega^{(4\epsilon)}(\mathbf{x}), \quad \mathbf{x} \in \Omega. \quad (33)$$

After that, substituting the above residual functions into the multi-scale fourth-order PDE (1) respectively, the residual equations for the second-order multi-scale solution, third-order multi-scale solution and fourth-order

multi-scale solution are derived as follows.

$$\left\{ \begin{aligned} & \frac{\partial^2}{\partial x_i \partial x_j} \left[ D_{ijkl}^\epsilon(\mathbf{x}) \frac{\partial^2 Z_\Delta^{(2\epsilon)}(\mathbf{x})}{\partial x_k \partial x_l} \right] \\ & \quad = -\epsilon^{-1}(B_1\omega^{(2)} + B_2\omega^{(1)} + B_3\omega^{(0)}) \\ & \quad \quad - \epsilon^0(B_2\omega^{(2)} + B_3\omega^{(1)} + B_4\omega^{(0)} - q) \\ & \quad \quad - \epsilon(B_3\omega^{(2)} + B_4\omega^{(1)}) - \epsilon^2 B_4\omega^{(2)} := \epsilon^{-1}E_2(\mathbf{x}, \mathbf{y}), \text{ in } \Omega, \\ & Z_\Delta^{(2\epsilon)}(\mathbf{x}) = -\epsilon^2\omega^{(2)}(\mathbf{x}, \mathbf{y}) := \epsilon^2\chi_2(\mathbf{x}), \text{ on } \partial\Omega, \\ & \frac{\partial Z_\Delta^{(2\epsilon)}(\mathbf{x})}{\partial x_j} \hat{n}_j = \frac{\partial \omega^\epsilon(\mathbf{x})}{\partial x_j} \hat{n}_j - \frac{\partial \omega^{(2\epsilon)}(\mathbf{x})}{\partial x_j} \hat{n}_j := \epsilon I_{2j}(\mathbf{x}) \hat{n}_j, \text{ on } \partial\Omega. \end{aligned} \right. \quad (34)$$

$$\left\{ \begin{aligned} & \frac{\partial^2}{\partial x_i \partial x_j} \left[ D_{ijkl}^\epsilon(\mathbf{x}) \frac{\partial^2 Z_\Delta^{(3\epsilon)}(\mathbf{x})}{\partial x_k \partial x_l} \right] \\ & \quad = -\epsilon^0(B_1\omega^{(3)} + B_2\omega^{(2)} + B_3\omega^{(1)} + B_4\omega^{(0)} - q) \\ & \quad \quad - \epsilon(B_2\omega^{(3)} + B_3\omega^{(2)} + B_4\omega^{(1)}) - \epsilon^2(B_3\omega^{(3)} + B_4\omega^{(2)}) \\ & \quad \quad - \epsilon^3 B_4\omega^{(3)} := \epsilon^0 E_3(\mathbf{x}, \mathbf{y}), \text{ in } \Omega, \\ & Z_\Delta^{(3\epsilon)}(\mathbf{x}) = -\epsilon^2\omega^{(2)}(\mathbf{x}, \mathbf{y}) - \epsilon^3\omega^{(3)}(\mathbf{x}, \mathbf{y}) := \epsilon^2\chi_3(\mathbf{x}), \text{ on } \partial\Omega, \\ & \frac{\partial Z_\Delta^{(3\epsilon)}(\mathbf{x})}{\partial x_j} \hat{n}_j = \frac{\partial \omega^\epsilon(\mathbf{x})}{\partial x_j} \hat{n}_j - \frac{\partial \omega^{(3\epsilon)}(\mathbf{x})}{\partial x_j} \hat{n}_j := \epsilon I_{3j}(\mathbf{x}) \hat{n}_j, \text{ on } \partial\Omega. \end{aligned} \right. \quad (35)$$

$$\left\{ \begin{aligned} & \frac{\partial^2}{\partial x_i \partial x_j} \left[ D_{ijkl}^\epsilon(\mathbf{x}) \frac{\partial^2 Z_\Delta^{(4\epsilon)}(\mathbf{x})}{\partial x_k \partial x_l} \right] \\ & \quad = -\epsilon(B_1\omega^{(4)} + B_2\omega^{(3)} + B_3\omega^{(2)} + B_4\omega^{(1)}) \\ & \quad \quad - \epsilon^2(B_2\omega^{(4)} + B_3\omega^{(3)} + B_4\omega^{(2)}) \\ & \quad \quad - \epsilon^3(B_3\omega^{(4)} + B_4\omega^{(3)}) - \epsilon^4 B_4\omega^{(4)} := \epsilon E_4(\mathbf{x}, \mathbf{y}), \text{ in } \Omega, \\ & Z_\Delta^{(4\epsilon)}(\mathbf{x}) = -\epsilon^2\omega^{(2)}(\mathbf{x}, \mathbf{y}) - \epsilon^3\omega^{(3)}(\mathbf{x}, \mathbf{y}) - \epsilon^4\omega^{(4)}(\mathbf{x}, \mathbf{y}) := \epsilon^2\chi_4(\mathbf{x}), \text{ on } \partial\Omega, \\ & \frac{\partial Z_\Delta^{(4\epsilon)}(\mathbf{x})}{\partial x_j} \hat{n}_j = \frac{\partial \omega^\epsilon(\mathbf{x})}{\partial x_j} \hat{n}_j - \frac{\partial \omega^{(4\epsilon)}(\mathbf{x})}{\partial x_j} \hat{n}_j := \epsilon I_{4j}(\mathbf{x}) \hat{n}_j, \text{ on } \partial\Omega. \end{aligned} \right. \quad (36)$$

Analyzing the residual equations (34) and (35), we can clearly find that second-order multi-scale solution and third-order multi-scale solution fail to preserve local mechanical balance due to the error terms  $O(\epsilon^{-1})$  and  $O(\epsilon^0)$  in their right sides with the quantitative relationship  $\epsilon^{-1} \ll \epsilon^0 \ll \epsilon$ . In

contrast, the error term of fourth-order multi-scale solution in the residual equation (36) shall preserve the local mechanical balance and provide the high-accuracy performance when  $\epsilon$  is a small constant. Additionally, when the microstructural parameter  $\epsilon \rightarrow 0$ , the right-hand error term of the residual equation (36) also tends to zero, indicating that the proposed fourth-order multi-scale solution  $\omega^{(4\epsilon)}$  converges to the exact solution  $\omega^\epsilon$  in a local point-wise sense. This capability is the primary impetus for current study to develop the FOMS solution manifesting high-fidelity computation performance for composite Kirchhoff plates.

### 3.2. Global error estimate in the energy sense

To the best of our knowledge, the following error estimate has been established for fourth-order Kirchhoff plate model in [35].

$$\|\omega^\epsilon(\mathbf{x})\|_{H^2(\Omega)} \leq C_\Omega \|q(\mathbf{x})\|_{H^{-2}(\Omega)} + C_\Omega \|g_1(\mathbf{x})\|_{H^{3/2}(\Omega)} + C_\Omega \|g_2(\mathbf{x})\|_{H^{1/2}(\Omega)}. \quad (37)$$

However, this error estimate can not be employed to obtain the explicit error order for fourth-order multi-scale solution  $\omega^{(4\epsilon)}$  with residual equation (36). The reason is that the appearance of  $\epsilon^{-2}$ -order terms lead to an order reduction phenomenon when using trace theorem to  $\|\epsilon^2 \chi_4(\mathbf{x})\|_{H^{3/2}(\Omega)}$ , which makes it impossible to obtain an explicit error estimate.

In order to an explicit error estimate for fourth-order multi-scale solution  $\omega^{(4\epsilon)}$ , we need to present some assumptions as follows.

- (B<sub>1</sub>) Suppose  $\Omega \subset \mathbb{R}^2$  is a bounded convex domain and a union of integral unit cells, i.e.  $\bar{\Omega} = \cup_{\mathbf{z} \in I_\epsilon} \epsilon(\mathbf{z} + \bar{\mathbf{Y}})$ , where the index set  $I_\epsilon = \{\mathbf{z} = (z_1, z_2) \in Z^2, \epsilon(\mathbf{z} + \bar{\mathbf{Y}}) \subset \bar{\Omega}\}$ . Besides, let  $E_{\mathbf{z}} = \epsilon(\mathbf{z} + \mathbf{Y})$  be the translational unit cell and  $\partial E_{\mathbf{z}}$  be its boundary with  $E_{\mathbf{z}} = \ell_1 \cup \ell_2 \cup \ell_3 \cup \ell_4$ , as shown in Fig. 1.
- (B<sub>2</sub>) The stiffness function  $D_{ijkl}(\mathbf{y})$  is piecewise constants on the microscopic PUC  $\mathbf{Y}$ .
- (B<sub>3</sub>) Define  $\Delta_1$  and  $\Delta_2$  to be middle hyperplanes on the microscopic PUC  $\mathbf{Y}$ , and assume that the microscopic PUC  $\mathbf{Y}$  is geometrically symmetric with respect to  $\Delta_1$  and  $\Delta_2$ , as exhibited in Fig. 1.

**Lemma 1.** Define the differential operator  $\sigma_{\mathbf{Y}}(\Phi) = \hat{n}_i \frac{\partial}{\partial y_j} [D_{ijkl}(\mathbf{y}) \frac{\partial^2 \Phi}{\partial y_k \partial y_l}]$ , and under the assumptions (A<sub>1</sub>)-(A<sub>2</sub>) and (B<sub>2</sub>)-(B<sub>3</sub>), it can be proven that  $\sigma_{\mathbf{Y}}(\mathcal{N}_2^{\alpha_1 \alpha_2})$  is continuous on the boundary  $E_{\mathbf{z}}$ .

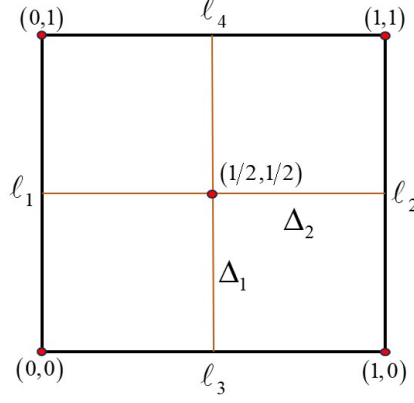


Figure 1: The symmetry and boundaries of microscopic PUC  $\mathbf{Y}$ .

**Proof :** Inspired by the references [15, 16, 37] and the definition (16) of second-order cell function  $\mathcal{N}_2^{\alpha_1\alpha_2}$ , we define the following two functions.

$$\Lambda_1^{\alpha_1\alpha_2}(\mathbf{y}) = \frac{\partial}{\partial y_j} \left[ D_{1jkl}(\mathbf{y}) \frac{\partial^2 \mathcal{N}_2^{\alpha_1\alpha_2}(\mathbf{y})}{\partial y_k \partial y_l} \right] + \frac{\partial D_{1j\alpha_1\alpha_2}(\mathbf{y})}{\partial y_j}, \quad (38)$$

$$\Lambda_2^{\alpha_1\alpha_2}(\mathbf{y}) = \frac{\partial}{\partial y_j} \left[ D_{2jkl}(\mathbf{y}) \frac{\partial^2 \mathcal{N}_2^{\alpha_1\alpha_2}(\mathbf{y})}{\partial y_k \partial y_l} \right] + \frac{\partial D_{2j\alpha_1\alpha_2}(\mathbf{y})}{\partial y_j}. \quad (39)$$

Then, we can derive the following equality according to the definition (16).

$$\frac{\partial \Lambda_1^{\alpha_1\alpha_2}(\mathbf{y})}{\partial y_1} + \frac{\partial \Lambda_2^{\alpha_1\alpha_2}(\mathbf{y})}{\partial y_2} = 0. \quad (40)$$

Furthermore, we set the test function  $v(\mathbf{y}) = (e^{i2\pi m_1 y_1} - 1)(e^{i2\pi m_2 y_2} - 1)$ ,  $m_1 \neq 0$ ,  $m_2 \neq 0$ . Next, employing the assumptions (B<sub>2</sub>)-(B<sub>3</sub>), and the same approach in references [15, 16, 37], and defining  $v_1(\mathbf{y}) = e^{i2\pi m_2 y_2} - 1$  and  $v_2(\mathbf{y}) = e^{i2\pi m_1 y_1} - 1$ , it follows that

$$\int_{\mathbf{Y}} \left( \frac{\partial \Lambda_1^{\alpha_1\alpha_2}(\mathbf{y})}{\partial y_1} + \frac{\partial \Lambda_2^{\alpha_1\alpha_2}(\mathbf{y})}{\partial y_2} \right) v_1(\mathbf{y}) d\mathbf{Y} = \int_{\ell_1} [\Lambda_1^{\alpha_1\alpha_2}(\mathbf{y})] v_1(\mathbf{y}) ds = 0, \quad (41)$$

$$\int_{\mathbf{Y}} \left( \frac{\partial \Lambda_1^{\alpha_1\alpha_2}(\mathbf{y})}{\partial y_1} + \frac{\partial \Lambda_2^{\alpha_1\alpha_2}(\mathbf{y})}{\partial y_2} \right) v_2(\mathbf{y}) d\mathbf{Y} = \int_{\ell_3} [\Lambda_2^{\alpha_1\alpha_2}(\mathbf{y})] v_2(\mathbf{y}) ds = 0, \quad (42)$$

where  $[\Lambda_1^{\alpha_1\alpha_2}(\mathbf{y})]$  and  $[\Lambda_2^{\alpha_1\alpha_2}(\mathbf{y})]$  denotes the jump of the functions  $\Lambda_1^{\alpha_1\alpha_2}(\mathbf{y})$  and  $\Lambda_2^{\alpha_1\alpha_2}(\mathbf{y})$ , respectively. Moreover, by virtue of the completeness of the

function families  $\{e^{i2\pi m_1 y_1}\}_{m_1=-\infty}^{+\infty}$  and  $\{e^{i2\pi m_2 y_2}\}_{m_2=-\infty}^{+\infty}$ , it can be derived that  $[\Lambda_1^{\alpha_1 \alpha_2}(\mathbf{y})]_{\ell_1} = 0$  and  $[\Lambda_2^{\alpha_1 \alpha_2}(\mathbf{y})]_{\ell_3} = 0$ .

Moreover, the following two equalities can be easily obtained

$$\int_{\mathbf{Y}} \left( \frac{\partial \Lambda_1^{\alpha_1 \alpha_2}(\mathbf{y})}{\partial y_1} + \frac{\partial \Lambda_2^{\alpha_1 \alpha_2}(\mathbf{y})}{\partial y_2} \right) d\mathbf{Y} = \int_{\ell_1} [\Lambda_1^{\alpha_1 \alpha_2}(\mathbf{y})] ds + \int_{\ell_3} [\Lambda_2^{\alpha_1 \alpha_2}(\mathbf{y})] ds = 0. \quad (43)$$

$$\int_{\mathbf{Y}} \left( \frac{\partial \Lambda_1^{\alpha_1 \alpha_2}(\mathbf{y})}{\partial y_1} + \frac{\partial \Lambda_2^{\alpha_1 \alpha_2}(\mathbf{y})}{\partial y_2} \right) d\mathbf{Y} = \int_{\ell_1} [\sigma_{\mathbf{Y}}(\mathcal{N}_2^{\alpha_1 \alpha_2})] ds + \int_{\ell_3} [\sigma_{\mathbf{Y}}(\mathcal{N}_2^{\alpha_1 \alpha_2})] ds = 0. \quad (44)$$

Hence, we can deduce that  $\sigma_{\mathbf{Y}}(\mathcal{N}_2^{\alpha_1 \alpha_2})] ds + \int_{\ell_3} [\sigma_{\mathbf{Y}}(\mathcal{N}_2^{\alpha_1 \alpha_2})]$  is continuous on  $E_{\mathbf{z}}$  on the basis of  $[\Lambda_1^{\alpha_1 \alpha_2}(\mathbf{y})]_{\ell_1} = 0$  and  $[\Lambda_2^{\alpha_1 \alpha_2}(\mathbf{y})]_{\ell_3} = 0$ .

**Lemma 2.** *Under the assumptions  $(A_1)$ – $(A_2)$  and  $(B_2)$ – $(B_3)$ , it can be proven that  $\sigma_{\mathbf{Y}}(\mathcal{N}_3^{\alpha_1 \alpha_2 \alpha_3})$  and  $\sigma_{\mathbf{Y}}(\mathcal{N}_4^{\alpha_1 \alpha_2 \alpha_3 \alpha_4})$  are continuous on the boundary  $E_{\mathbf{z}}$ .*

**Proof :** Inspired by the same approach in references [15, 16, 37], the continuous property of  $\sigma_{\mathbf{Y}}(\mathcal{N}_3^{\alpha_1 \alpha_2 \alpha_3})$  and  $\sigma_{\mathbf{Y}}(\mathcal{N}_4^{\alpha_1 \alpha_2 \alpha_3 \alpha_4})$  can be proved.

**Lemma 3.** *Based on the lemmas 1 and 2, it can be proven that the first-order and second-order derivatives of all microscopic cell functions  $\mathcal{N}_2^{\alpha_1 \alpha_2}$ ,  $\mathcal{N}_3^{\alpha_1 \alpha_2 \alpha_3}$  and  $\mathcal{N}_4^{\alpha_1 \alpha_2 \alpha_3 \alpha_4}$  are continuous on the boundary  $E_{\mathbf{z}}$ .*

**Proof :** From the lemmas 1 and 2, we have acknowledged that the third-order derivatives of all microscopic cell functions are continuous on the boundary  $E_{\mathbf{z}}$ . Hence, it is no doubt that first-order and second-order derivatives of all microscopic cell functions are continuous on the boundary  $E_{\mathbf{z}}$ .

Based on the aforementioned assumptions and lemmas, we now present the ultimate result of global error estimate for the FOMS solution  $\omega^{(4\epsilon)}(\mathbf{x})$  of the fourth-order Kirchhoff plate equation (1) as the subsequent theorem.

**Theorem 2.** *Consider  $\omega^\epsilon(\mathbf{x})$  as the weak solution of multi-scale fourth-order equation (1), while  $\omega^{(0)}(\mathbf{x})$  represents the weak solution of corresponding homogenized equation (20). Let  $\omega^{(4\epsilon)}(\mathbf{x})$  denotes the FOMS solution given by formula (25). Assuming the above hypotheses  $(A_1)$ – $(A_3)$  and  $(B_1)$ – $(B_3)$  hold, we derive the subsequent global error estimation if  $\omega^{(0)}(\mathbf{x}) \in H^8(\Omega)$ .*

$$\|\omega^\epsilon(\mathbf{x}) - \omega^{(4\epsilon)}(\mathbf{x})\|_{H_0^2(\Omega)} \leq C_\Omega \epsilon. \quad (45)$$

Here  $C_\Omega$  is a positive constant dependent of  $\Omega$ , but irrespective of  $\epsilon$ .

**Proof :** The residual equation and associated boundary conditions in (36) are utilized to obtain the explicit error estimate (40). Firstly, multiplying both sides of the residual equation (36) by the test function  $Z_\Delta^{(4\epsilon)}(\mathbf{x})$  and using integration on  $\Omega$ , the following equation is obtained

$$\int_\Omega \frac{\partial^2}{\partial x_i \partial x_j} \left[ D_{ijkl}^\epsilon(\mathbf{x}) \frac{\partial^2 Z_\Delta^{(4\epsilon)}(\mathbf{x})}{\partial x_k \partial x_l} \right] Z_\Delta^{(4\epsilon)}(\mathbf{x}) d\Omega = \int_\Omega \epsilon E_4(\mathbf{x}, \mathbf{y}) Z_\Delta^{(4\epsilon)}(\mathbf{x}) d\Omega. \quad (46)$$

Immediately after applying Green's formula twice to the left term of equation (39), then we have

$$\begin{aligned} & \int_\Omega D_{ijkl}^\epsilon(\mathbf{x}) \frac{\partial^2 Z_\Delta^{(4\epsilon)}(\mathbf{x})}{\partial x_k \partial x_l} \frac{\partial^2 Z_\Delta^{(4\epsilon)}(\mathbf{x})}{\partial x_i \partial x_j} d\Omega \\ & + \int_{\partial\Omega} \frac{\partial}{\partial x_j} \left[ D_{ijkl}^\epsilon(\mathbf{x}) \frac{\partial^2 Z_\Delta^{(4\epsilon)}(\mathbf{x})}{\partial x_k \partial x_l} \right] Z_\Delta^{(4\epsilon)}(\mathbf{x}) \hat{n}_i ds \\ & - \int_{\partial\Omega} D_{ijkl}^\epsilon(\mathbf{x}) \frac{\partial^2 Z_\Delta^{(4\epsilon)}(\mathbf{x})}{\partial x_k \partial x_l} \frac{\partial Z_\Delta^{(4\epsilon)}(\mathbf{x})}{\partial x_i} \hat{n}_j ds \\ & + \sum_{\mathbf{z} \in I_\epsilon} \int_{\partial E_{\mathbf{z}}} \frac{\partial}{\partial x_j} \left[ D_{ijkl}^\epsilon(\mathbf{x}) \frac{\partial^2 Z_\Delta^{(4\epsilon)}(\mathbf{x})}{\partial x_k \partial x_l} \right] Z_\Delta^{(4\epsilon)}(\mathbf{x}) \hat{n}_i d\Gamma_{\mathbf{y}} \\ & - \sum_{\mathbf{z} \in I_\epsilon} \int_{\partial E_{\mathbf{z}}} D_{ijkl}^\epsilon(\mathbf{x}) \frac{\partial^2 Z_\Delta^{(4\epsilon)}(\mathbf{x})}{\partial x_k \partial x_l} \frac{\partial Z_\Delta^{(4\epsilon)}(\mathbf{x})}{\partial x_i} \hat{n}_j d\Gamma_{\mathbf{y}} \\ & = \int_\Omega \epsilon E_4(\mathbf{x}, \mathbf{y}) Z_\Delta^{(4\epsilon)}(\mathbf{x}) d\Omega, \end{aligned} \quad (47)$$

where the integral terms on  $\partial E_{\mathbf{z}}$  arise from employing Green's formula on interface  $\partial E_{\mathbf{z}}$  between two adjacent PUCs.

On recalling the assumption B<sub>1</sub> and the boundary conditions of microscopic cell functions, thus we can derive

$$Z_\Delta^{(4\epsilon)}(\mathbf{x}) = \epsilon^2 \chi_4(\mathbf{x}) = 0, \quad \text{on } \partial\Omega, \quad (48)$$

$$\frac{\partial Z_\Delta^{(4\epsilon)}(\mathbf{x})}{\partial x_j} \hat{n}_j = \epsilon I_{4j}(\mathbf{x}) \hat{n}_j = 0, \quad \text{on } \partial\Omega. \quad (49)$$



Considering the assumption B<sub>2</sub>, and the lemmas 1-3, thus we shall obtain

Furthermore, by means of the assumption B<sub>2</sub>, and the lemmas 1-3, it is not difficult to check that

$$\sum_{\mathbf{z} \in I_\epsilon} \int_{\partial E_{\mathbf{z}}} D_{ijkl}^\epsilon(\mathbf{x}) \frac{\partial^2 Z_\Delta^{(4\epsilon)}(\mathbf{x})}{\partial x_k \partial x_l} \frac{\partial Z_\Delta^{(4\epsilon)}(\mathbf{x})}{\partial x_i} \hat{n}_j d\Gamma_{\mathbf{y}} = 0. \quad (51)$$

Substituting the boundary conditions (41)-(44) into equation (40), thus equation (40) can be simplified as

$$\int_{\Omega} D_{ijkl}^\epsilon(\mathbf{x}) \frac{\partial^2 Z_\Delta^{(4\epsilon)}(\mathbf{x})}{\partial x_k \partial x_l} \frac{\partial^2 Z_\Delta^{(4\epsilon)}(\mathbf{x})}{\partial x_i \partial x_j} d\Omega = \int_{\Omega} \epsilon E_4(\mathbf{x}, \mathbf{y}) Z_\Delta^{(4\epsilon)}(\mathbf{x}) d\Omega. \quad (52)$$

Furthermore, on the basis of assumptions A<sub>1</sub>-A<sub>3</sub>, and the priori estimate (37) of fourth-order equation, the following inequality holds

$$\left\| Z_\Delta^{(4\epsilon)}(\mathbf{x}) \right\|_{H_0^2(\Omega)} \leq C_\Omega \|\epsilon E_4(\mathbf{x}, \mathbf{y})\|_{H^{-2}(\Omega)}. \quad (53)$$

Finally, we obtain that the explicit error estimate in the integral sense for the higher-order multi-scale solution of the fourth-order multi-scale plate problem (1) as below.

$$\left\| \omega^\epsilon(\mathbf{x}) - \omega^{(4\epsilon)}(\mathbf{x}) \right\|_{H_0^2(\Omega)} \leq C_\Omega \epsilon. \quad (54)$$

Hence the proof of Theorem 2 is complete.

#### 4. Multi-scale numerical algorithm

Based on the theoretical results established in the previous chapters, we now develop the multi-scale numerical algorithm for fourth-order Kirchhoff plate problem in composite plates (1). The detailed multi-scale algorithm is illustrated as below.

- Step 1. Identify the geometric configuration of PUC  $\mathbf{Y} = [0, 1]^2$  and generate a family of triangular finite element meshes  $\mathcal{T}_{h_1} = \{K\}$  for PUC  $\mathbf{Y}$ , where  $h_1 = \max_K \{h_K\}$ .
- Step 2. Define the Morley finite element space  $\mathbb{P}_{h_1}^2(\mathbf{Y})$  or Hsieh-Clough-Tocher (HCT) finite element space  $\mathbb{P}_{h_1}^{\text{HCT}}(\mathbf{Y})$  for solving auxiliary cell problems. Next, employ FEM to solve the second-order cell functions defined by (16) on  $\mathbb{P}_{h_1}^2(\mathbf{Y})$  or  $\mathbb{P}_{h_1}^{\text{HCT}}(\mathbf{Y})$ . Note that classical periodic boundary

condition of auxiliary cell problems is replaced by clamped boundary condition for practical numerical implementation. The detailed computational scheme with test function  $v^{h_1}(\mathbf{y}) \in \mathbb{P}_{h_1}^2(\mathbf{Y})/\mathbb{P}_{h_1}^{\text{HCT}}(\mathbf{Y})$  is establishes for solving second-order cell problems (16) as below.

$$\int_{\mathbf{Y}} D_{ijkl}(\mathbf{y}) \frac{\partial^2 \mathcal{N}_2^{\alpha_1 \alpha_2}(\mathbf{y})}{\partial y_k \partial y_l} \frac{\partial^2 v^{h_1}(\mathbf{y})}{\partial y_i \partial y_j} d\mathbf{Y} = - \int_{\mathbf{Y}} D_{ij\alpha_1 \alpha_2}(\mathbf{y}) \frac{\partial^2 v^{h_1}(\mathbf{y})}{\partial y_i \partial y_j} d\mathbf{Y}. \quad (55)$$

- Step 3. Employ FEM to solve the third-order cell functions defined by (19) on  $\mathbb{P}_{h_1}^2(\mathbf{Y})$  or  $\mathbb{P}_{h_1}^{\text{HCT}}(\mathbf{Y})$ .
- Step 4. Evaluate the homogenized bending stiffness parameters  $\hat{D}_{ijkl}$  at macro-scale based on the formula (21).
- Step 5. Identify the geometric configuration of the macroscopic region  $\Omega$  and  $\mathcal{T}_{h_0} = \{e\}$  be a family of triangular finite element meshes for the macroscopic region  $\Omega$ , where  $h_0 = \max_e \{h_e\}$ .
- Step 6. Define the Morley finite element space  $\mathbb{P}_{h_0}^2(\Omega)$  or HCT finite element space  $\mathbb{P}_{h_0}^{\text{HCT}}(\Omega)$  [38] for macroscopic homogenized Kirchhoff plate equation (20). The specific computational scheme with test function  $\phi^{h_0}(\mathbf{x}) \in \mathbb{P}_{h_0}^2(\Omega)/\mathbb{P}_{h_0}^{\text{HCT}}(\Omega)$  is establishes for macroscopic homogenized Kirchhoff plate equation (20).

$$\begin{cases} \int_{\Omega} \hat{D}_{ijkl} \frac{\partial^2 \omega^{(0)}(\mathbf{x})}{\partial x_k \partial x_l} \frac{\partial^2 \phi^{h_0}(\mathbf{x})}{\partial x_i \partial x_j} d\Omega = \int_{\Omega} q(\mathbf{x}) \phi^{h_0}(\mathbf{x}) d\Omega, \\ \omega^{(0)}(\mathbf{x}) = g_1(\mathbf{x}) \text{ on } \partial\Omega, \\ \frac{\partial \omega^{(0)}(\mathbf{x})}{\partial x_j} \hat{n}_j = g_2(\mathbf{x}) \text{ on } \partial\Omega. \end{cases} \quad (56)$$

- Step 7. Employ FEM to solve the fourth-order cell functions defined by (24) on  $\mathbb{P}_{h_1}^2(\mathbf{Y})$  or  $\mathbb{P}_{h_1}^{\text{HCT}}(\mathbf{Y})$ .
- Step 8. The average approach on relative elements is utilized to compute the spatial derivatives of macroscopic homogenized solution  $\omega^{(0)}(\mathbf{x})$  in [15, 16, 37, 39]. Furthermore, the fourth-order multi-scale solution  $\omega^{(4\epsilon)}(\mathbf{x})$  for transverse displacement field of composite Kirchhoff plates is computed by the formula (25).

## 5. Numerical experiments and results

This section presents several numerical examples to validate the computational accuracy and efficiency of the proposed FOMS methodology. The

numerical experiments are conducted on a HP desktop workstation equipped with an Intel Core i9-13900H processor (2.60 GHz) and 32.0 GB of internal memory, and all numerical simulations are performed based on Freefem++ software [40].

In addition, since it is scarcely impossible to obtain the exact solutions for the plate bending problems of composite Kirchhoff plates, we use the direct numerical simulation (DNS) solution  $\omega_D^\epsilon(\mathbf{x})$  as reference solution for evaluating the computational performance of the proposed FOMS approach. Furthermore, we denote some error notations  $e_0(\mathbf{x}) = \omega^0(\mathbf{x}) - \omega_{\text{DNS}}^\epsilon(\mathbf{x})$ ,  $e_2(\mathbf{x}) = \omega^{(2\epsilon)}(\mathbf{x}) - \omega_{\text{DNS}}^\epsilon(\mathbf{x})$ ,  $e_3(\mathbf{x}) = \omega^{(3\epsilon)}(\mathbf{x}) - \omega_{\text{DNS}}^\epsilon(\mathbf{x})$  and  $e_4(\mathbf{x}) = \omega^{(4\epsilon)}(\mathbf{x}) - \omega_{\text{DNS}}^\epsilon(\mathbf{x})$  for subsequent error analysis.

### 5.1. Validation of the computational performance of FOMS method

In this example, a composite thin plate with clamped boundary condition is investigated, whose multi-scale structure  $\Omega = (x_1, x_2) = [0, 1] \times [0, 1] \text{cm}^2$ , microscopic unit cell  $\mathbf{Y} = (y_1, y_2) = [0, 1] \times [0, 1]$  and macroscopic homogenization structure are depicted in Fig. 2. This composite plate with the characteristic periodic parameter  $\epsilon = 1/8$  consists of two component materials, where Young's modulus and Poisson's ratio of the matrix material (yellow color) are 50.0GPa and 0.20, respectively. For the inclusion material (red color), these values are 8.0MPa and 0.20. In addition, the transverse load imposed on this composite plate is set to 1500.0N/cm<sup>2</sup>.

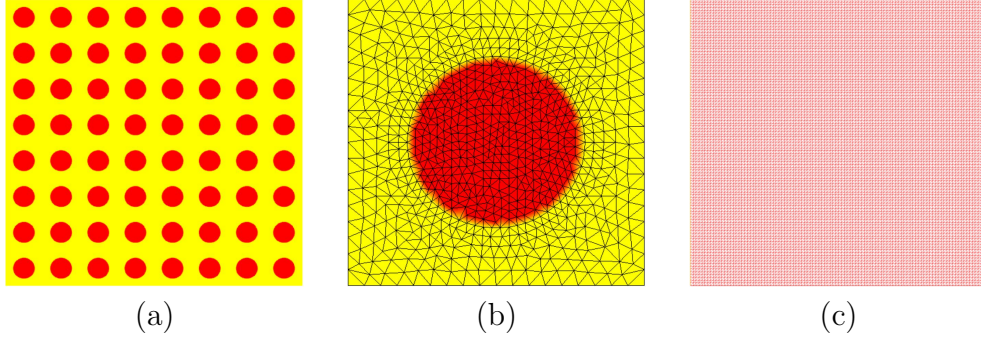


Figure 2: (a) The multi-scale structure of composite plate  $\Omega$ ; (b) the microscopic unit cell  $\mathbf{Y}$ ; (c) the macroscopic homogenization structure.

Next, the proposed FOMS computational method based on Morley finite element and HCT finite element is employed to simulate this composite

Kirchhoff plate. Table 1 presents the detail comparison of computational resource cost of the FOMS method and reference direct numerical simulation.

Table 1: Comparison of computational cost.

	Multi-scale problem	Cell problem	Homogenized problem
Number of elements	209920	1620	21632
Number of nodes	105361	847	11025
	Direct numerical simulation		Multi-scale algorithm
Time/Morley	10.419s		7.594s
Time/HCT	91.642s		20.552s

Furthermore, Table 2 displays the detailed computational accuracy comparison of the FOMS method and reference direct numerical simulation.

Table 2: Comparison of computational accuracy.

Morley	$\frac{\ e_0\ _{L^2}}{\ \omega_D^\epsilon\ _{L^2}}$	$\frac{\ e_2\ _{L^2}}{\ \omega_D^\epsilon\ _{L^2}}$	$\frac{\ e_3\ _{L^2}}{\ \omega_D^\epsilon\ _{L^2}}$	$\frac{\ e_4\ _{L^2}}{\ \omega_D^\epsilon\ _{L^2}}$	$\frac{ e_0 _{H^1}}{ \omega_D^\epsilon _{H^1}}$	$\frac{ e_2 _{H^1}}{ \omega_D^\epsilon _{H^1}}$	$\frac{ e_3 _{H^1}}{ \omega_D^\epsilon _{H^1}}$	$\frac{ e_4 _{H^1}}{ \omega_D^\epsilon _{H^1}}$
	Percentage %	5.001	4.854	4.858	1.464	56.760	56.375	56.346
HCT	$\frac{\ e_0\ _{L^2}}{\ \omega_D^\epsilon\ _{L^2}}$	$\frac{\ e_2\ _{L^2}}{\ \omega_D^\epsilon\ _{L^2}}$	$\frac{\ e_3\ _{L^2}}{\ \omega_D^\epsilon\ _{L^2}}$	$\frac{\ e_4\ _{L^2}}{\ \omega_D^\epsilon\ _{L^2}}$	$\frac{ e_0 _{H^1}}{ \omega_D^\epsilon _{H^1}}$	$\frac{ e_2 _{H^1}}{ \omega_D^\epsilon _{H^1}}$	$\frac{ e_3 _{H^1}}{ \omega_D^\epsilon _{H^1}}$	$\frac{ e_4 _{H^1}}{ \omega_D^\epsilon _{H^1}}$
	Percentage %	4.845	4.718	4.722	1.565	56.346	55.986	55.957

Figs. 3 and 4 are plotted to visualize the simulative results for solutions  $\omega^{(0)}$ ,  $\omega^{(2\epsilon)}$ ,  $\omega^{(3\epsilon)}$ ,  $\omega^{(4\epsilon)}$  and  $\omega_D^\epsilon$  based on Morley finite element and HCT finite element, respectively.

Beside, Figs. 5-8 display the simulative results for the numerical gradients of solutions  $\omega^{(0)}$ ,  $\omega^{(2\epsilon)}$ ,  $\omega^{(3\epsilon)}$ ,  $\omega^{(4\epsilon)}$  and  $\omega_D^\epsilon$  based on Morley finite element and HCT finite element, respectively.

As plainly shown in Table 1, the FOMS approach proposed herein demonstrates a substantial reduction in computational resource, particularly in terms of CPU memory and time, when contrasted with high-resolution DNS. Specifically, the proposed FOMS approach achieves an approximate saving of 27.11% and 77.57% in computational time when employing Morley and HCT finite elements, respectively. Furthermore, the numerical accuracy analysis in Table 2 clearly illustrates that the FOMS solution achieves a significant

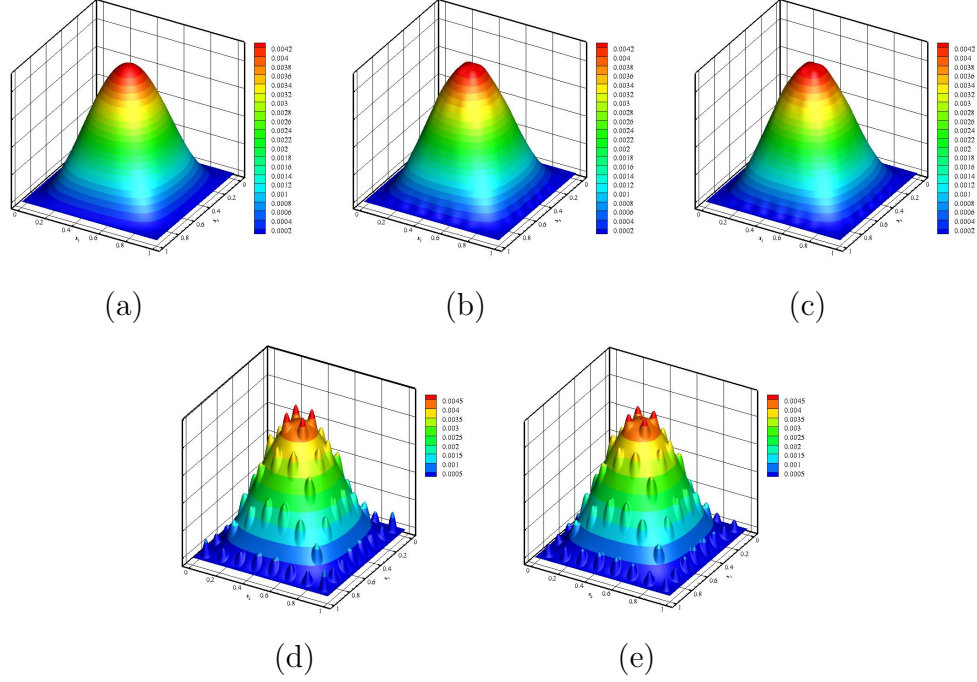


Figure 3: The transverse displacement of composite Kirchhoff plate computed by Morley finite element: (a)  $\omega^{(0)}$ ; (b)  $\omega^{(2\epsilon)}$ ; (c)  $\omega^{(3\epsilon)}$ ; (d)  $\omega^{(4\epsilon)}$ ; (e)  $\omega_D^\epsilon$ .

enhancement in computational accuracy compared with macroscopic homogenized solution, second-order multi-scale solution and third-order multi-scale solution, especially for  $H^1$  semi-norm. Moreover, we can conclude that the computational efficiency and accuracy of the FOMS approach based on Morley finite element is superior to those of FOMS approach based on HCT finite element. Similarly, the computational results in Figs. 3 and 4 also demonstrate only FOMS solution have the capacity to accurately capture the highly microscopic oscillation of composite thin plate, and the computational accuracy of macroscopic homogenized, second-order and third-order solutions is significantly inferior. Additionally, the numerical results in Figs. 5-8 demonstrate the proposed FOMS method can accurately capture the gradient behaviors of composite thin plate. In addition, the numerical error observed in the gradient results from the HCT element at the plate boundary, when using the same mesh, are likely due to inaccurate computation of higher-order derivatives for the macroscopic homogenized solution. Hence, the FOMS method based on Morley finite element is employed to the numerical simu-

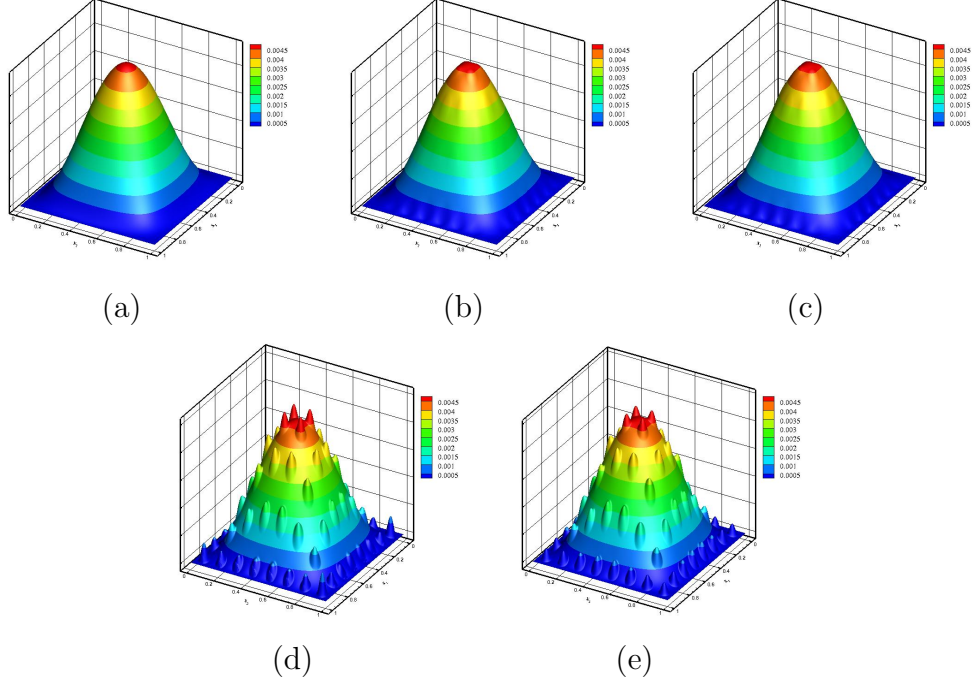


Figure 4: The transverse displacement of composite Kirchhoff plate computed by HCT finite element: (a)  $\omega^{(0)}$ ; (b)  $\omega^{(2\epsilon)}$ ; (c)  $\omega^{(3\epsilon)}$ ; (d)  $\omega^{(4\epsilon)}$ ; (e)  $\omega_D^\epsilon$ .

lation in the subsequent numerical examples.

### 5.2. Application to composite Kirchhoff plates with different kinds of inclusions

In this example, other four kinds of composite Kirchhoff plates with clamped boundary condition are simulated, whose geometric configurations of microscopic PUCs are illustrated in Fig. 9. The investigated composite plates with the characteristic periodic parameter  $\epsilon = 1/8$  are composed of two constituent materials. And the Young's modulus and Poisson's ratio of the matrix material are 60.0GPa and 0.35, respectively. For the inclusion material, these values are 2.4MPa and 0.35. In addition, the transverse load imposed on this composite plate is set to 2500.0N/cm<sup>2</sup>.

Based on the conclusion in subsection 5.1, the FOMS method based on Morley finite element is employed in this subsection. After numerical simulation, Table 3 shows the computational accuracy of the proposed FOMS

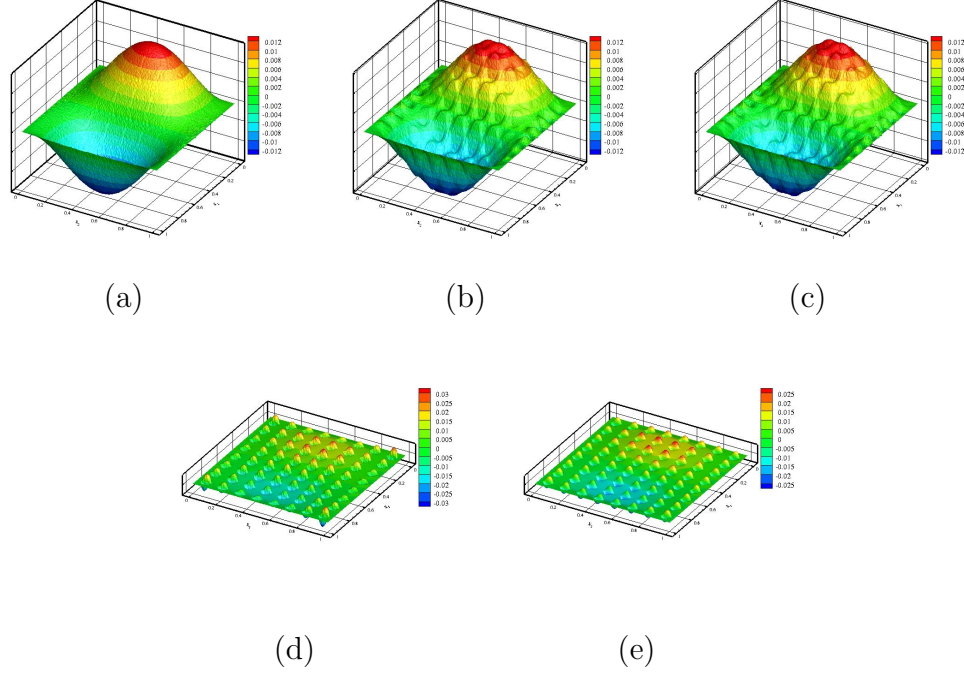


Figure 5: The  $x_1$ -direction gradient of transverse displacement of composite Kirchhoff plate computed by Morley finite element: (a)  $\frac{\partial \omega^{(0)}}{\partial x_1}$ ; (b)  $\frac{\partial \omega^{(2\epsilon)}}{\partial x_1}$ ; (c)  $\frac{\partial \omega^{(3\epsilon)}}{\partial x_1}$ ; (d)  $\frac{\partial \omega^{(4\epsilon)}}{\partial x_1}$ ; (e)  $\frac{\partial \omega_D^\epsilon}{\partial x_1}$ .

method based on Morley finite element for composite Kirchhoff plates with four kinds of microscopic PUCs.

Furthermore, Figs. 10-13 display the numerical results for solutions  $\omega^{(0)}$ ,  $\omega^{(2\epsilon)}$ ,  $\omega^{(3\epsilon)}$ ,  $\omega^{(4\epsilon)}$  and  $\omega_D^\epsilon$  based on Morley finite element of composite Kirchhoff plates with four kinds of microscopic PUCs, respectively.

As shown in Table 3, it can be clearly found that the FOMS approach exhibits the optimal numerical accuracy for highly oscillating behaviors of four kinds of composite Kirchhoff plates, compared with macroscopic homogenized, second-order multi-scale and third-order multi-scale approaches. In addition, it can be obviously seen from Figs. 10-13 that the FOMS solutions for four kinds of composite Kirchhoff plates agree well with those of direct numerical simulation on highly refined meshes. In stark contrast, the macroscopic homogenized solution can merely reflect the macroscopic bending behavior of the composite plates, while the second- and third-order



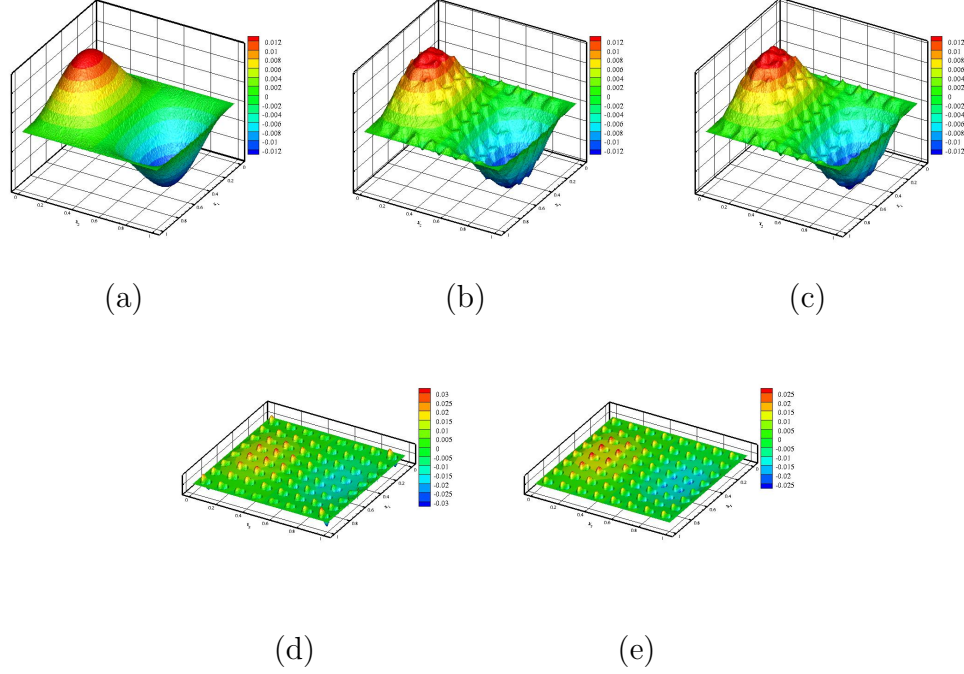


Figure 6: The  $x_2$ -direction gradient of transverse displacement of composite Kirchhoff plate computed by Morley finite element: (a)  $\frac{\partial \omega^{(0)}}{\partial x_2}$ ; (b)  $\frac{\partial \omega^{(2\epsilon)}}{\partial x_2}$ ; (c)  $\frac{\partial \omega^{(3\epsilon)}}{\partial x_2}$ ; (d)  $\frac{\partial \omega^{(4\epsilon)}}{\partial x_2}$ ; (e)  $\frac{\partial \omega_D^\epsilon}{\partial x_2}$ .

multi-scale solutions can capture the inadequate local information at the micro-scale.

We should highlight that another potential advantage of the introduced FOMS methodology is its applicability to the effective computation of large-scale composite plates with a vast number of unit cells. In order to validate this advanced strength, the proposed FOMS methodology is utilized to compute the bending behaviors of the aforementioned four kinds of composite Kirchhoff plates with the characteristic periodic parameter  $\epsilon = 1/16$ , as shown in Fig. 14.

Moreover, the transverse displacement of four kinds of composite Kirchhoff plates with a large amount of PUCs is shown in Fig. 15. At this time, the Freefem++ software is unable to access the high-resolution reference solutions due to a highly refined mesh. However, the proposed FOMS method enables accurate and efficient computation of these fourth-order multi-scale

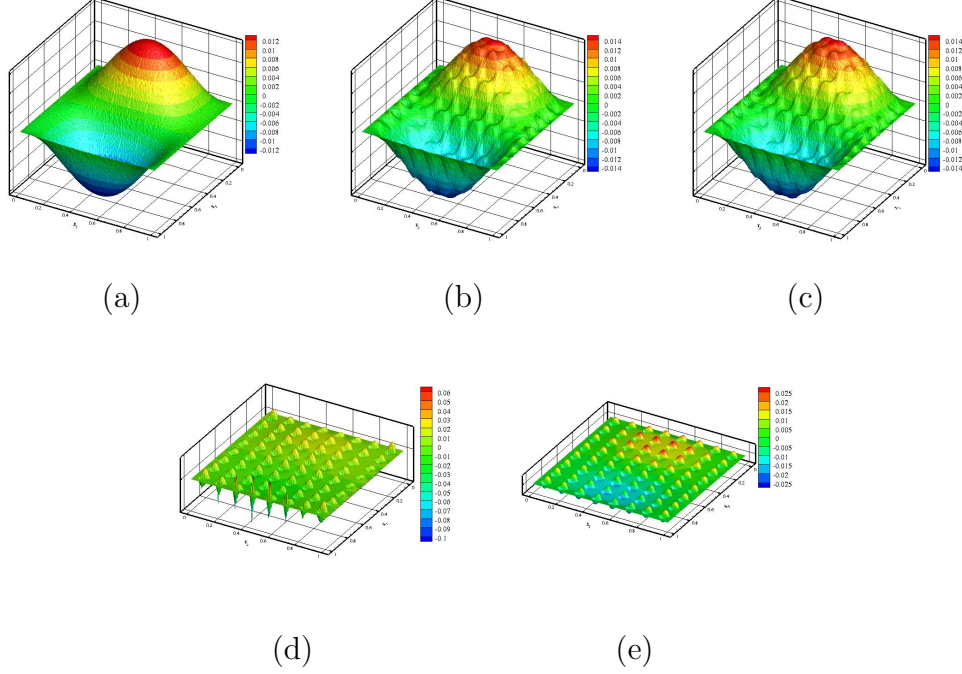


Figure 7: The  $x_1$ -direction gradient of transverse displacement of composite Kirchhoff plate computed by HCT finite element: (a)  $\frac{\partial \omega^{(0)}}{\partial x_1}$ ; (b)  $\frac{\partial \omega^{(2\epsilon)}}{\partial x_1}$ ; (c)  $\frac{\partial \omega^{(3\epsilon)}}{\partial x_1}$ ; (d)  $\frac{\partial \omega^{(4\epsilon)}}{\partial x_1}$ ; (e)  $\frac{\partial \omega_D^\epsilon}{\partial x_1}$ .

problems with highly spatial heterogeneities.

In real-world engineering applications, it is impractical to obtain reference FEM solutions for large-scale composite plates due to prohibitive computational overhead. However, the FOMS method can effectively simulate large-scale composite plates with minimal computational resource consumption. Also, the proposed FOMS approach is robust for simulating the composite plates with massive PUCs without increasing the computational overhead, which is of great engineering values.

## 6. Conclusions and outlooks

Owing to the key properties of being lightweight, high-strength, and enabling large structural spans, composite plates have abroad application in the aerospace, construction, and machinery industries, etc. However, analytical approaches are prohibitively difficult to obtain an exact solution of

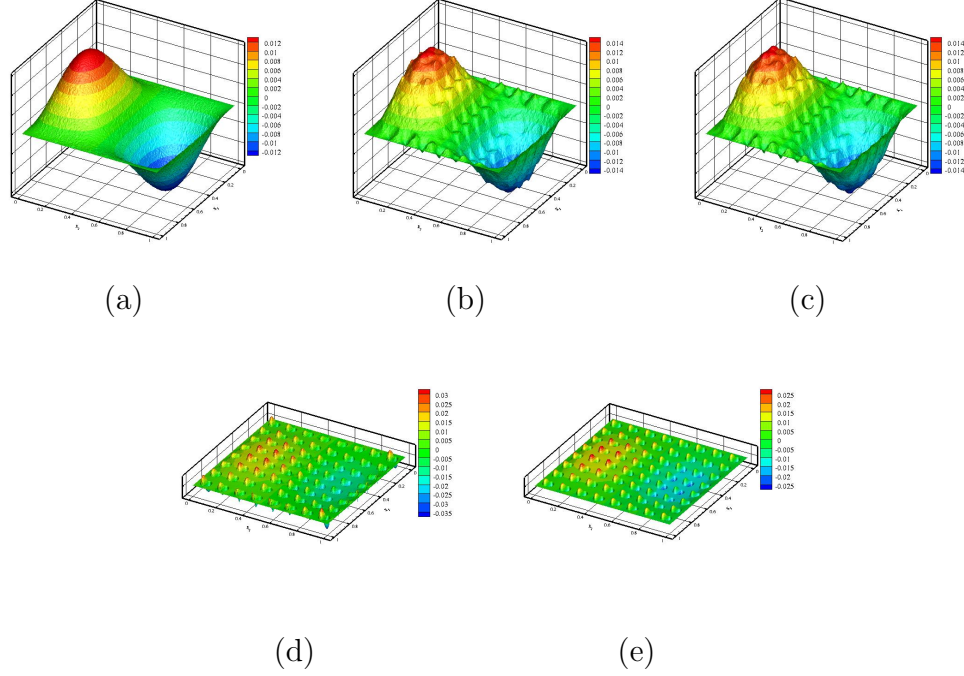


Figure 8: The  $x_2$ -direction gradient of transverse displacement of composite Kirchhoff plate computed by HCT finite element: (a)  $\frac{\partial \omega^{(0)}}{\partial x_2}$ ; (b)  $\frac{\partial \omega^{(2\epsilon)}}{\partial x_2}$ ; (c)  $\frac{\partial \omega^{(3\epsilon)}}{\partial x_2}$ ; (d)  $\frac{\partial \omega^{(4\epsilon)}}{\partial x_2}$ ; (e)  $\frac{\partial \omega_D^\epsilon}{\partial x_2}$ .

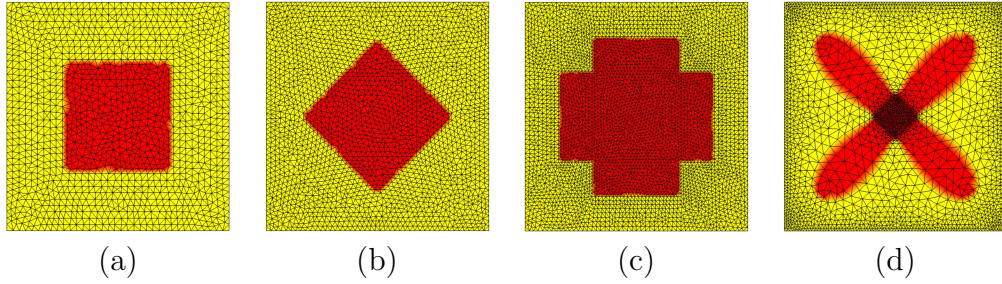


Figure 9: Four kinds of composite Kirchhoff plates: (a) type-I PUC  $\mathbf{Y}$ ; (b) type-II PUC  $\mathbf{Y}$ ; (c) type-III PUC  $\mathbf{Y}$ ; (d) type-IV PUC  $\mathbf{Y}$ .

fourth-order composite Kirchhoff plate models with rapidly oscillating and highly discontinuous coefficients. Moreover, direct simulation by classical numerical methods involves a substantial computational cost. Hence, the development of accurate and efficient multi-scale method is essential for ef-

Table 3: Comparison of computational accuracy.

FOMS-Morley	$\frac{\ e_0\ _{L^2}}{\ \omega_D^\epsilon\ _{L^2}}$	$\frac{\ e_2\ _{L^2}}{\ \omega_D^\epsilon\ _{L^2}}$	$\frac{\ e_3\ _{L^2}}{\ \omega_D^\epsilon\ _{L^2}}$	$\frac{\ e_4\ _{L^2}}{\ \omega_D^\epsilon\ _{L^2}}$	$\frac{ e_0 _{H^1}}{ \omega_D^\epsilon _{H^1}}$	$\frac{ e_2 _{H^1}}{ \omega_D^\epsilon _{H^1}}$	$\frac{ e_3 _{H^1}}{ \omega_D^\epsilon _{H^1}}$	$\frac{ e_4 _{H^1}}{ \omega_D^\epsilon _{H^1}}$
Type-I/Percentage %	9.937	9.893	9.897	2.733	87.058	86.856	86.829	21.630
Type-II/Percentage %	10.864	10.690	10.693	3.495	85.233	85.009	84.985	19.425
Type-III/Percentage %	19.570	19.442	19.445	5.693	93.222	93.090	93.069	22.923
Type-IV/Percentage %	1.495	1.031	1.015	0.345	29.887	26.199	25.710	8.586

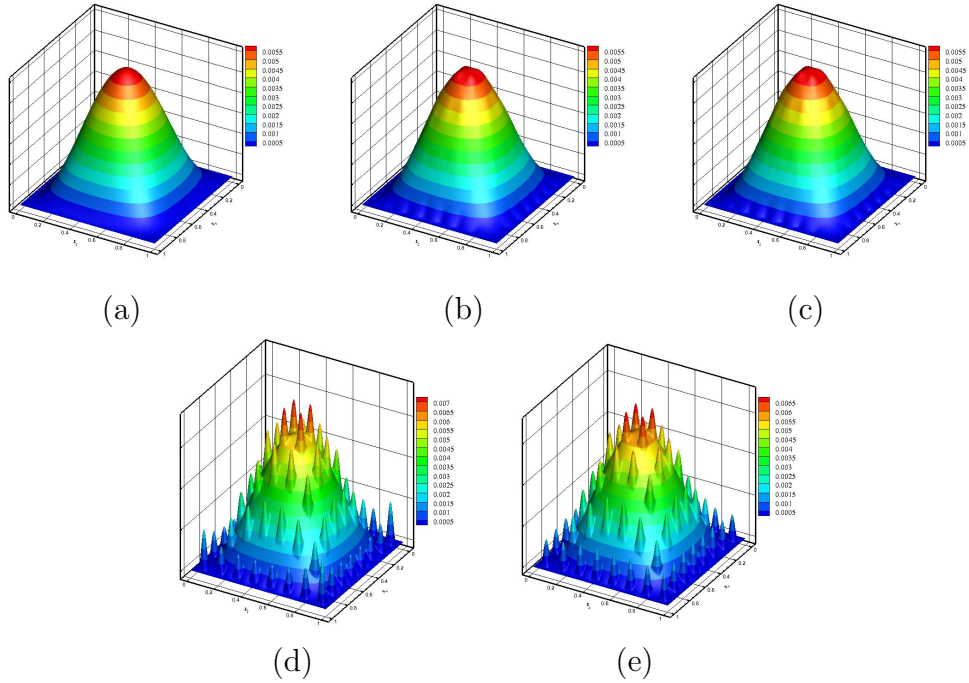


Figure 10: The transverse displacement of composite Kirchhoff plate with type-I PUC computed by Morley finite element: (a)  $\omega^{(0)}$ ; (b)  $\omega^{(2\epsilon)}$ ; (c)  $\omega^{(3\epsilon)}$ ; (d)  $\omega^{(4\epsilon)}$ ; (e)  $\omega_D^\epsilon$ .

fectively investigating the mechanical behavior of composite plate structures, offering significant scientific insights and practical applications.

This study proposes a novel fourth-order multi-scale method (fourth-order multi-scale computational model and numerical algorithm), which paves the way for simulating the composite Kirchhoff plates both accurately and efficiently. The innovations of this work are threefold: high-accuracy FOMS computational model with novel fourth-order correctors, local and global error analyses for validating the local balance preserving and proving the

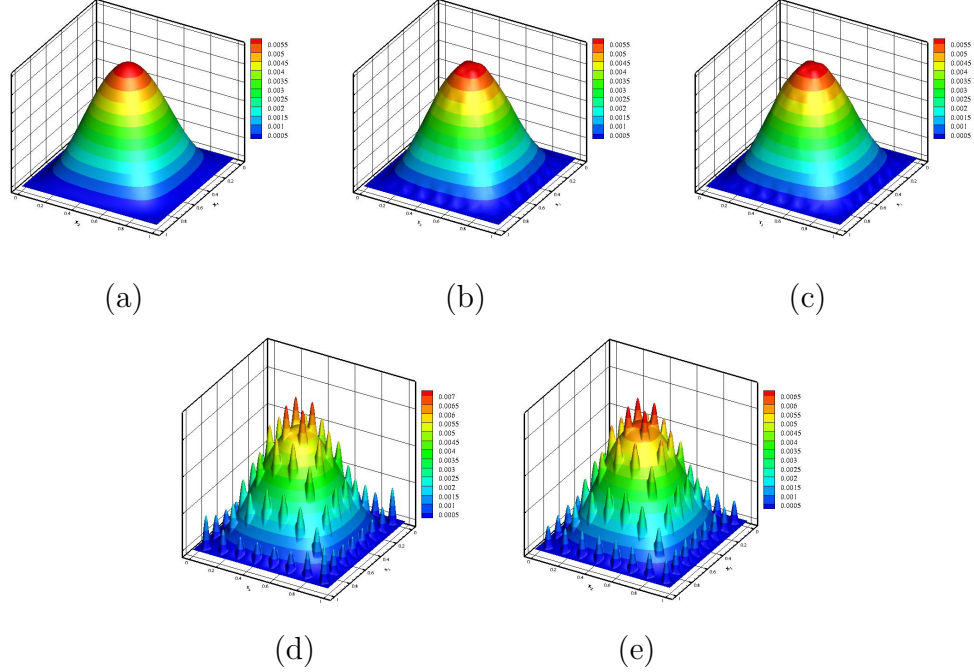


Figure 11: The transverse displacement of composite Kirchhoff plate with type-II PUC computed by Morley finite element: (a)  $\omega^{(0)}$ ; (b)  $\omega^{(2\epsilon)}$ ; (c)  $\omega^{(3\epsilon)}$ ; (d)  $\omega^{(4\epsilon)}$ ; (e)  $\omega_D^\epsilon$ .

explicit convergence, efficient numerical algorithm with reduced computational resource. Furthermore, numerical experiments clearly demonstrated that the proposed FOMS methodology with local balance preserving can accurately capture the highly oscillating behavior of composite plates and provide high-fidelity numerical solutions for engineering applications. Also, the fourth-order multi-scale method owns excellent agreement between its theoretical framework and numerical results. Furthermore, numerical experiments also illustrate the proposed FOMS method can strongly economize the computer resource compared with finite element method. These computational advantages are of great application value for large-scale engineering simulation.

In the future, the introduced FOMS method will extend to simulate the dynamic vibration problem of composite Kirchhoff plates. Additionally, the FOMS approach will focus on the extension to composite plate considering three-scale, nonlinear and nonlocal mechanical behaviors.

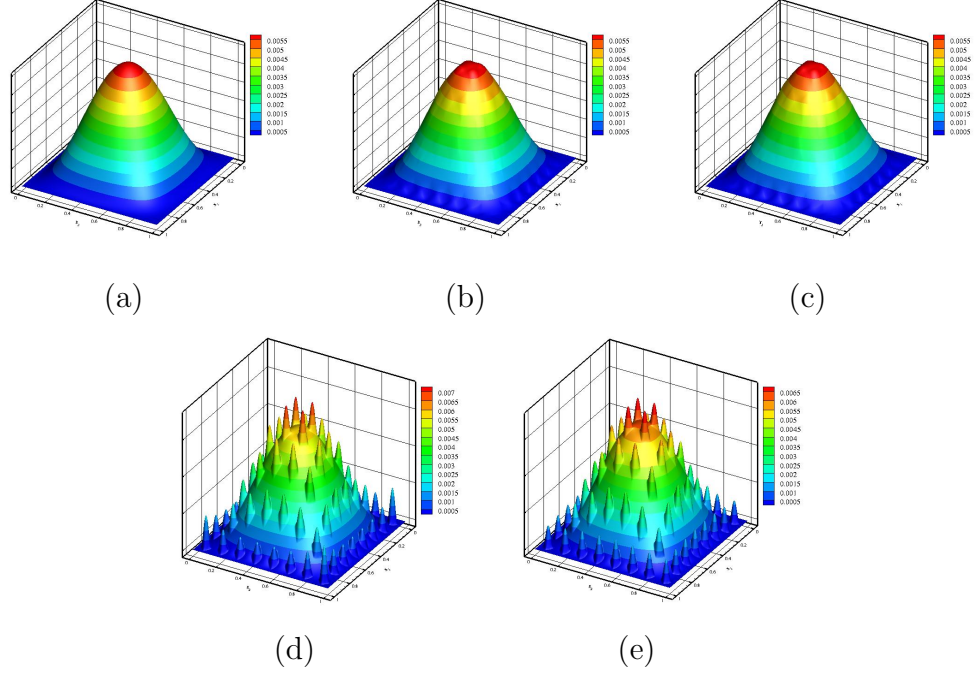


Figure 12: The transverse displacement of composite Kirchhoff plate with type-III PUC computed by Morley finite element: (a)  $\omega^{(0)}$ ; (b)  $\omega^{(2\epsilon)}$ ; (c)  $\omega^{(3\epsilon)}$ ; (d)  $\omega^{(4\epsilon)}$ ; (e)  $\omega_D^\epsilon$ .

## Acknowledgments

This research was supported by the National Natural Science Foundation of China (No. 12471387), Xidian University Specially Funded Project for Interdisciplinary Exploration (No. TZJH2024008), Fundamental Research Funds for the Central Universities (No. QTZX25082), and also supported by the High-Performance Computing Platform of Xidian University.

## References

- [1] T. Lewinski, J. J. Telega, Plates, laminates and shells: asymptotic analysis and homogenization, volume 52, World Scientific, 2000.
- [2] D. Cioranescu, P. Donato, An introduction to homogenization, Oxford university press, 1999.
- [3] O. A. Oleĭnik, A. Shamaev, G. Yosifian, Mathematical problems in elasticity and homogenization, volume 26, Elsevier, 1992.



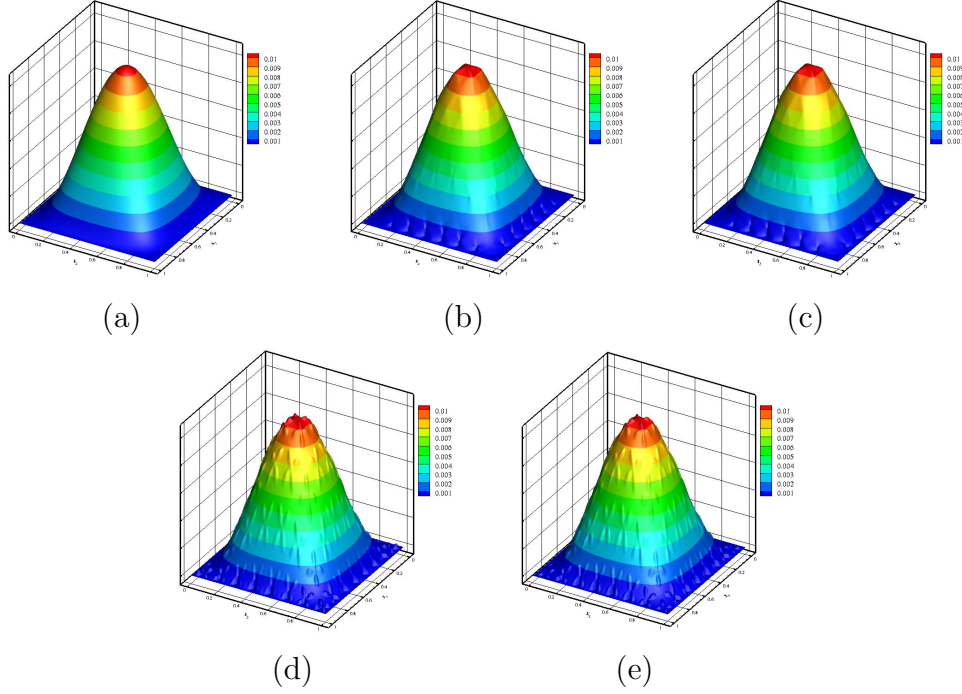


Figure 13: The transverse displacement of composite Kirchhoff plate with type-IV PUC computed by Morley finite element: (a)  $\omega^{(0)}$ ; (b)  $\omega^{(2\epsilon)}$ ; (c)  $\omega^{(3\epsilon)}$ ; (d)  $\omega^{(4\epsilon)}$ ; (e)  $\omega_D^\epsilon$ .

- [4] T. Hou, X.-H. Wu, Z. Cai, Convergence of a multiscale finite element method for elliptic problems with rapidly oscillating coefficients, *Mathematics of Computation* 68 (1999) 913–943.
- [5] Y. Efendiev, T. Y. Hou, *Multiscale finite element methods: theory and applications*, volume 4, Springer Science & Business Media, 2009.
- [6] A. Abdulle, E. Weinan, B. Engquist, E. Vanden-Eijnden, The heterogeneous multiscale method, *Acta Numerica* 21 (2012) 1–87.
- [7] T. J. Hughes, Multiscale phenomena: Green’s functions, the dirichlet-to-neumann formulation, subgrid scale models, bubbles and the origins of stabilized methods, *Computer Methods in Applied Mechanics and Engineering* 127 (1995) 387–401.
- [8] Y. Xing, Y. Yang, X. Wang, A multiscale eigenelement method and its

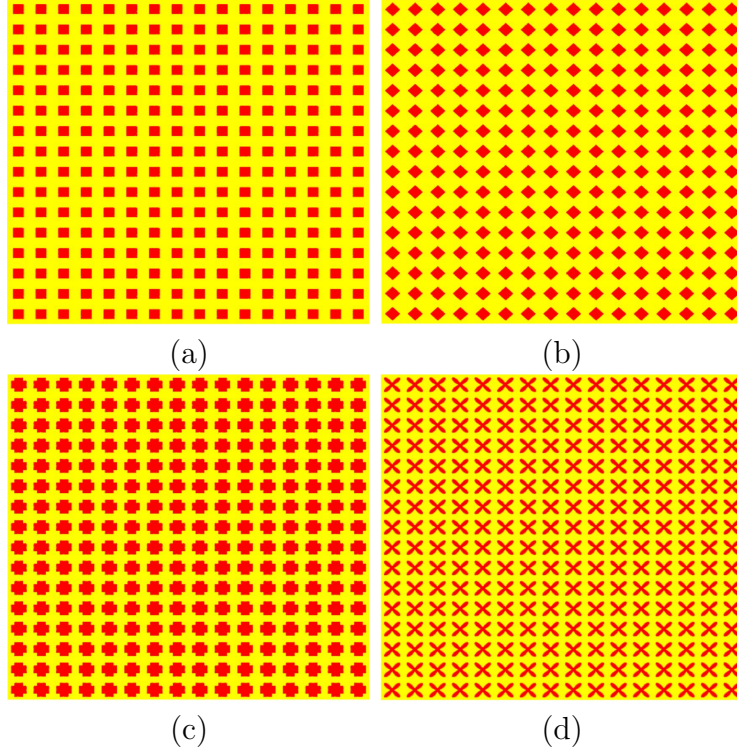


Figure 14: Four kinds of composite Kirchhoff plates with  $\epsilon = 1/16$ : (a) type-I PUC  $\mathbf{Y}$ ; (b) type-II PUC  $\mathbf{Y}$ ; (c) type-III PUC  $\mathbf{Y}$ ; (d) type-IV PUC  $\mathbf{Y}$ .

application to periodical composite structures, *Composite Structures* 92 (2010) 2265–2275.

- [9] P. Henning, A. Målqvist, Localized orthogonal decomposition techniques for boundary value problems, *SIAM Journal on Scientific Computing* 36 (2014) A1609–A1634.
- [10] Y. Efendiev, J. Galvis, T. Y. Hou, Generalized multiscale finite element methods (gmsfem), *Journal of computational physics* 251 (2013) 116–135.
- [11] E. T. Chung, Y. Efendiev, W. T. Leung, Constraint energy minimizing generalized multiscale finite element method, *Computer Methods in Applied Mechanics and Engineering* 339 (2018) 298–319.
- [12] H. Dong, J. Cui, Y. Nie, Z. Yang, Q. Ma, X. Cheng, Multiscale computa-



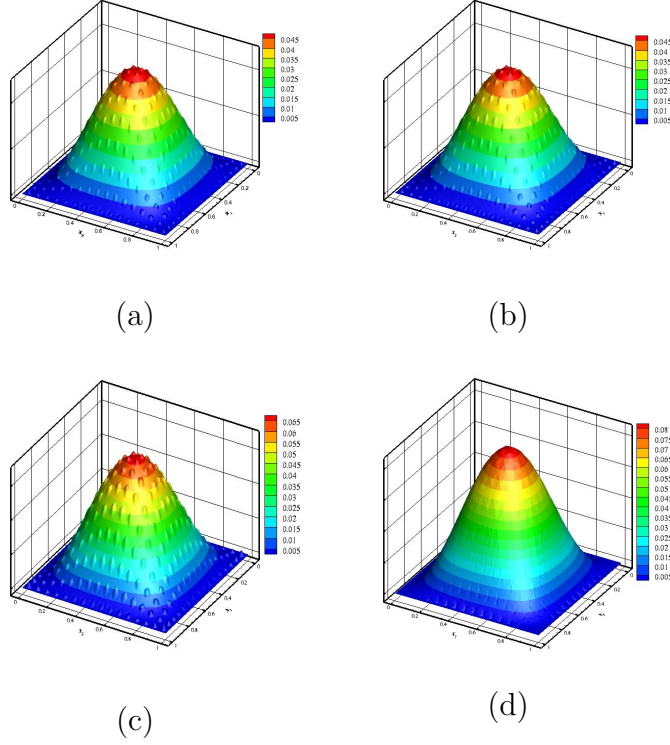


Figure 15: The transverse displacement of four kinds of composite Kirchhoff plates with  $\epsilon = 1/16$  computed by Morley finite element: (a) type-I PUC  $\mathbf{Y}$ ; (b) type-II PUC  $\mathbf{Y}$ ; (c) type-III PUC  $\mathbf{Y}$ ; (d) type-IV PUC  $\mathbf{Y}$ .

tional method for transient heat conduction problems of periodic porous materials with diverse periodic configurations in different subdomains, *Applied Numerical Mathematics* 136 (2019) 215–234.

- [13] H. Dong, J. Cui, Y. Nie, K. Jin, X. Guan, Z. Yang, High-order three-scale computational method for elastic behavior analysis and strength prediction of axisymmetric composite structures with multiple spatial scales, *Mathematics and Mechanics of Solids* 26 (2021) 905–936.
- [14] H. Dong, X. Guan, Y. Nie, Multiscale method and convergence analysis for coupled nonlinear thermomechanical problems in heterogeneous shells, *SIAM Journal on Scientific Computing* 47 (2025) B190–B219.
- [15] L.-Q. Cao, J.-Z. Cui, D.-C. Zhu, Multiscale asymptotic analysis and nu-

- merical simulation for the second order helmholtz equations with rapidly oscillating coefficients over general convex domains, *SIAM Journal on Numerical Analysis* 40 (2002) 543–577.
- [16] L.-Q. Cao, J.-Z. Cui, Asymptotic expansions and numerical algorithms of eigenvalues and eigenfunctions of the dirichlet problem for second order elliptic equations in perforated domains, *Numerische Mathematik* 96 (2004) 525–581.
  - [17] S. E. Pastukhova, Estimates in homogenization of higher-order elliptic operators, *Applicable Analysis* 95 (2016) 1449–1466.
  - [18] S. Pastukhova, Operator error estimates for homogenization of fourth order elliptic equations, *St. Petersburg Mathematical Journal* 28 (2017) 273–289.
  - [19] T. Suslina, Homogenization of the dirichlet problem for higher-order elliptic equations with periodic coefficients, *St. Petersburg Mathematical Journal* 29 (2018) 325–362.
  - [20] T. Suslina, Homogenization of the neumann problem for higher order elliptic equations with periodic coefficients, *Complex Variables and Elliptic Equations* 63 (2018) 1185–1215.
  - [21] W. Niu, Z. Shen, Y. Xu, Convergence rates and interior estimates in homogenization of higher order elliptic systems, *Journal of Functional Analysis* 274 (2018) 2356–2398.
  - [22] W. Niu, Y. Xu, Uniform boundary estimates in homogenization of higher-order elliptic systems, *Annali di Matematica Pura ed Applicata* (1923-) 198 (2019) 97–128.
  - [23] Y. Xu, W. Niu, Convergence rates in almost-periodic homogenization of higher-order elliptic systems, *Asymptotic Analysis* 123 (2021) 95–137.
  - [24] Z. Huang, Y. Xing, Y. Gao, Two-scale asymptotic homogenization method for composite kirchhoff plates with in-plane periodicity, *Aerospace* 9 (2022) 751.
  - [25] Z. Huang, X. Zeng, C. Wang, C. Liu, Two-scale convergence analysis and numerical simulation for periodic kirchhoff plates, *Heliyon* 11 (2025).

- [26] A. Kolpakov, Variational principles for stiffnesses of a non-homogeneous plate, *Journal of the Mechanics and Physics of Solids* 47 (1999) 2075–2092.
- [27] T.-S. Lok, Q.-H. Cheng, Elastic stiffness properties and behavior of truss-core sandwich panel, *Journal of Structural Engineering* 126 (2000) 552–559.
- [28] N. Buannic, P. Cartraud, T. Quesnel, Homogenization of corrugated core sandwich panels, *Composite structures* 59 (2003) 299–312.
- [29] Y. Cai, L. Xu, G. Cheng, Novel numerical implementation of asymptotic homogenization method for periodic plate structures, *International Journal of Solids and Structures* 51 (2014) 284–292.
- [30] B. Dong, C. Li, D. Wang, C.-T. Wu, Consistent multiscale analysis of heterogeneous thin plates with smoothed quadratic hermite triangular elements, *International Journal of Mechanics and Materials in Design* 12 (2016) 539–562.
- [31] M. Ren, J. Cong, B. Wang, X. Guo, Extended multiscale finite element method for small-deflection analysis of thin composite plates with aperiodic microstructure characteristics, *Composite Structures* 160 (2017) 422–434.
- [32] H. Li, Z. Sharif Khodaei, M. Aliabadi, Fft-based homogenisation for efficient concurrent multiscale modelling of thin plate structures, *Computational Mechanics* 75 (2025) 637–653.
- [33] Q. Li, J. Soric, T. Jarak, S. N. Atluri, A locking-free meshless local petrov–galerkin formulation for thick and thin plates, *Journal of Computational Physics* 208 (2005) 116–133.
- [34] J. Huang, X. Huang, Y. Xu, Convergence of an adaptive mixed finite element method for kirchhoff plate bending problems, *SIAM journal on numerical analysis* 49 (2011) 574–607.
- [35] L. Wang, X. Xu, *The Mathematical Basis of Finite Element Method*, Science Press, 2004.

- [36] K. Feng, Z. Shi, The Mathematical Theory of Elastic Structures, Science Press, 2010.
- [37] L.-Q. Cao, Multiscale asymptotic expansion and finite element methods for the mixed boundary value problems of second order elliptic equation in perforated domains, *Numerische Mathematik* 103 (2006) 11–45.
- [38] X. Shen, R. Wu, S. Zhu, Numerical method for two-dimensional linearly elastic clamped plate model, *International Journal of Computer Mathematics* 100 (2023) 1779–1793.
- [39] J. Cui, Multiscale computational method for unified design of structure, components and their materials, *Proceedings on Computational Mechanics in Science and Engineering, CCCM-2001*, Guangzhou (2001) 5–8.
- [40] F. Hecht, New development in freefem++, *Journal of numerical mathematics* 20 (2012) 1–14.